Batteries & Supercaps

Review
doi.org/10.1002/batt.202300594

Chemistry Europe
European Chemical Societies Publishing

www.batteries-supercaps.org

Short-Term Tests, Long-Term Predictions – Accelerating Ageing Characterisation of Lithium-Ion Batteries

Sabine Paarmann,*[a, c, h, k] Markus Schreiber,[b] Ahmed Chahbaz,[c, h] Felix Hildenbrand,[c, h] Gereon Stahl,[c, h] Marcel Rogge,[d] Philipp Dechent,[c, h, l] Oliver Queisser,[a] Sebastian Dominic Frankl,[e] Pablo Morales Torricos,[f] Yao Lu,[g] Nikolay I. Nikolov,[g] Maria Kateri,[g] Dirk Uwe Sauer,[c, h, i, j] Michael A. Danzer,[e] Thomas Wetzel,[a] Christian Endisch,[f] Markus Lienkamp,[b] Andreas Jossen,[d] and Meinert Lewerenz[f]

For the battery industry, quick determination of the ageing behaviour of lithium-ion batteries is important both for the evaluation of existing designs as well as for R&D on future technologies. However, the target battery lifetime is 8–10 years, which implies low ageing rates that lead to an unacceptably long ageing test duration under real operation conditions. Therefore, ageing characterisation tests need to be accelerated to obtain ageing patterns in a period ranging from a few weeks to a few months. Known strategies, such as increasing the severity of stress factors, for example, temperature, current, and taking measurements with particularly high precision, need care in application to achieve meaningful results. We observe that this challenge does not receive enough attention in typical ageing studies. Therefore, this review introduces the definition and challenge of accelerated ageing along existing methods to accelerate the characterisation of battery ageing and lifetime modelling. We systematically discuss approaches along the existing literature. In this context, several test conditions and feasible acceleration strategies are highlighted, and the underlying modelling and statistical perspective is provided. This makes the review valuable for all who set up ageing tests, interpret ageing data, or rely on ageing data to predict battery lifetime.

1. Introduction

Lithium-ion batteries (LIBs) have been the technology for mass-produced battery electric vehicles in the last decade.[1] Long operating times of more than 1 million miles (1.6 million km) and over two decades[2,3] are expected to be possible with a conservative cell design. However, the increase in energy density is often accompanied by reduced durability, which is why ensuring sufficient longevity is of particular interest. Although such long lifetimes are already achieved, economic competition demands much faster integration of new technical developments. The usual vehicle development process from early stages to the start of production takes about three years.[4] To be compatible with those product development time frames,

[a] Dr.-Ing. S. Paarmann, O. Queisser, Prof. T. Wetzel
Institute of Thermal Process Engineering (TVT), Karlsruhe Institute of Technology (KIT), Germany
E-mail: sabine.paarmann@gmail.com

[b] M. Schreiber, Prof. M. Lienkamp
School of Engineering & Design, Institute of Automotive Technology, Technical University of Munich, Germany

[c] Dr.-Ing. S. Paarmann, A. Chahbaz, F. Hildenbrand, G. Stahl, Dr.-Ing. P. Dechent, Prof. D. U. Sauer
Chair for Electrochemical Energy Conversion and Storage Systems, Institute for Power Electronics and Electrical Drives (ISEA), RWTH Aachen University, CampusBoulevard 89, 52074 Aachen, Germany

[d] M. Rogge, Prof. A. Jossen
Chair of Electrical Energy Storage Technology, Department of Energy and Process Engineering, TUM School of Engineering and Design, Technical University of Munich, Germany

[e] S. D. Frankl, Prof. M. A. Danzer
Chair of Electrical Energy Systems, University of Bayreuth, Germany

[f] P. Morales Torricos, Prof. C. Endisch, Dr. M. Lewerenz
Research Group Electromobility and Learning Systems, THI Ingolstadt, Germany

[g] Y. Lu, Dr. N. I. Nikolov, Prof. M. Kateri
Institute of Statistics, RWTH Aachen University, Germany

[h] Dr.-Ing. S. Paarmann, A. Chahbaz, F. Hildenbrand, G. Stahl, Dr.-Ing. P. Dechent, Prof. D. U. Sauer
Jülich Aachen Research Alliance, JARA-Energy, Templergraben 55, 52056 Aachen, Germany

[i] Prof. D. U. Sauer
Institute for Power Generation and Storage Systems (PGS), E.ON ERC, RWTH Aachen University, Mathieustrasse 10, 52074 Aachen, Germany

[j] Prof. D. U. Sauer
Helmholtz Institute Muenster (HI MS), IEK-12, Forschungszentrum Juelich, 52425 Jülich, Germany

[k] Dr.-Ing. S. Paarmann
Present Address: Department of Mechanical Engineering, Imperial College London, Exhibition Rd, South Kensington, London SW7 2AZ, UK

[l] Dr.-Ing. P. Dechent
Present Address: Department of Engineering Science, University of Oxford, Parks Road, Oxford OX1 3PJ, UK

the LIB design needs to be evaluated in just a few months or even less.[5] However, in terms of lifetime, reliable characterisation requires up to over a year of testing or even longer. In addition, a lifetime estimation of LIBs is necessary at an early stage of product development to underpin design decisions and qualify long-term application performance, especially as the LIB accounts for the largest part of the cost[6] of a battery electric vehicle. Thus, ageing characterisation requires acceleration to match the different time scales of product development, operating time and ageing rates of LIBs.

The goal of accelerated lifetime investigation can be summarised as characterising ageing, i.e. identifying and quantifying it, in a short period of time. In general, there are two strategies to achieve this goal. The first is to increase the accuracy of the measurement to quickly detect even the smallest degradation without accelerating the *ageing mechanisms* themselves. This is referred to as high precision measurement (HPM). The second strategy is to accelerate the *ageing mechanisms* and to make the degradation proceed faster by intensifying stress factors during operation, such as temperature or applied current. We refer to this in the following as accelerated ageing method (AAM).

Combining these two test strategies with a model, ranging from a simple linear extrapolation to more sophisticated approaches, enables lifetime performance prognoses of LIBs. Thus, the time-limiting factor, especially for industry, is the duration of the experiments using AAM and / or HPM. This will be addressed in this review, together with important issues to consider during testing. Thereby, three key questions arise:

1. What is the minimum duration of a test to capture the relevant reversible and irreversible effects with a certain level of accuracy?
2. What are the promising test strategies, and what are the limitations of a specific test strategy, for example extreme stress factors?
3. How do we model the accelerated ageing aiming at reliable and fast predictions that can be transferred to normal operating conditions?

As the lifetime and degradation of lithium-ion batteries are highly relevant, there is published work that addresses ageing mechanisms and ageing effects at the cell or system level[7–11] and ageing-related test methods.[12–14] Furthermore, there are reviews on specific stress factors,[15–18] as well as operation[19] and fast charging strategies.[20,21] However, to the best of our knowledge, there is no work reviewing the literature with a special focus on methods for accelerating the ageing characterisation. We hereby concentrate on the cell level, while ageing on the module or system level is out of the scope of this review.

The review is structured as follows. In Section 2, we provide definitions and basic terminologies of battery ageing and accelerated ageing characterisation with respect to an unaccelerated reference case. In Section 3, various characterisation methods are presented and compared. General remarks on cell characterisation are provided in Section 3.1. Different test strategies for calendar and cycle life tests are discussed later. Associated methods, ranging from high-precision tests to post-mortem analysis, are discussed regarding their ability to achieve a fast and reliable ageing characterisation in Sections 3.2 to 3.4. This includes the risk assessment of accelerating ageing tests to trigger additional ageing mechanisms and a critical analysis of acceleration limits. In Section 3.5, the review concludes with a modelling and statistical perspective, analysing the estimation and prediction precision of the proposed models as a function of the experiment duration and the number of cells tested.

2. Definitions

In the literature, there is no uniform use of terms regarding the ageing characterisation of lithium-ion cells. In the current state-of-the-art, many definitions are used synonymously or contrarily. Section 2 explains important principles and defines relevant terms to establish a common understanding. When a new term is introduced, it will be highlighted in bold and in italics. Subsequently, they are accentuated in italics. Table 1 conclusively summarises the introduced terminologies.

2.1. Definition of Ageing

Commonly, ageing is defined as a decrease in usable capacity or energy and an increase in impedance, further denoted as ***ageing effects***. The current battery condition relative to the pristine state is quantified by the state of health (SoH), whereby an SoH of 100 % indicates the pristine condition. During service life, ageing is reflected by an alteration of the SoH. Once a predefined threshold for usable capacity and resistance is exceeded, a cell has reached its end of life (EoL). The EoL for mobile applications, such as battery electric vehicles, is usually defined with 70 to 80 % remaining capacity[22–27] or 150 to 200 % internal resistance,[22,25] depending on the manufacturer and the use case's requirements.

During lifetime tests, ageing is typically tracked over time and charge throughput. A standard measure for the latter is the number of equivalent full cycles (EFCs), defined as the total amount of charge throughput related to the initial or nominal capacity of the cells of a complete charge and discharge cycle under standard conditions at beginning of life (BoL). We refer to time and charge throughput as ***ageing variables*** since they act as a reference with the progress of battery ageing. The observable *ageing effects* originate from various chemical and physical mechanisms from the molecular to the macroscopic level.[7,9,28] These mechanisms, subsequently called ***ageing mechanisms***, depend on the operating conditions to which the battery is exposed.

The operating conditions, for example, the applied current, cell temperature, depth of discharge (DoD) or intermediate idle periods, are denoted as ***stress factors***. These factors affect the cell electrically, thermally, chemically, and mechanically, thus determining its degradation. Hence, different *stress factors* or their combinations trigger different *ageing mechanisms*, which occur during battery operation (cyclic ageing), as well as during idle periods (calendar ageing). The *ageing rate* can be

Table 1. Definitions related to the accelerated ageing characterisation of LIB.

Defined terms	**explanations and associated variable/aspect**	**level**
stress factors	SoC, DoD, temperature, C-rate, continuous cycling	operational level
unaccelerated reference	load condition as in the application without acceleration	
acceleration techniques	accelerated ageing method (AAM) high precision measurement (HPM)	
sweet spot	highest consistent *ageing rate* in the accelerated test referring to the unaccelerated reference	
ageing mechanisms	lithium plating, transition metal dissolution, SEI formation	phenomenological level
degradation modes	loss of lithium inventory (LLI), loss of active material (LAM)	
ageing effects	capacity decrease, resistance increase	
irreversible ageing	ageing effects due to degradation modes	
reversible ageing	reversible ageing effects that are not referred to degradation modes (e.g. anode overhang effect)	
apparent ageing	superimposed reversible and irreversible ageing effects	
ageing trends	linear or progressive curve trends	
ageing rate	velocity or intensity of the occurring degradation	
ageing variables	charge throughput (e.g. EFC) and time	
reference performance test (RPT)	characterisation of the cell condition during ageing test to quantify ageing effects	
model conception	effect modelling, model-based extrapolation, statistical modelling	modelling level
transferability	comparability of unaccelerated reference and accelerated experiment	transmission level
consistency	similarity of the ageing effects and degradation modes	

interpreted as the velocity or intensity with which ageing progresses. The impact of stress factors on ageing will be reviewed and discussed in detail in Section 3.3.

In general, the ageing behaviour or ***ageing trend*** of a lithium-ion cell exhibits two sequences as indicated by the blue and red curve in Figure 1. Initially, the cells age with linear or approximately linear behaviour. During operation, several *ageing mechanisms* might act simultaneously, and thus the cell condition could change. As a result, the dominant mechanism can vary throughout service life, causing a transition in the *ageing trend*. Hence, a sudden, strongly nonlinear degradation might occur in the second stage. Such a transition is often called roll-over or knee point for progressive capacity fade and elbow for progressive resistance increase.[9,29–31] As schematically illustrated in Figure 1, initial degradation can occur at different *ageing rates*. This degradation rate depends on the applied stress factors and the cell chemistry examined.

Figure 1. Schematic *ageing trends* of lithium-ion batteries: low initial *ageing rate* with an early knee point (blue), moderate initial *ageing rate* with no knee point within the considered time frame (orange), high initial *ageing rate* with a late knee point (red).

Accelerated ageing characterisation aims to shorten the experiment duration by increasing this initial *ageing rate* or extrapolating the measured degradation based on a model. Hence, the accuracy and uncertainty of such predictions strongly depend on the progress of the test at which the forecast is made, with early predictions being more affected by the measurement error than later predictions. In addition, early predictions do not allow for an estimate of the continuously increasing ageing spread due to production-related cell-to-cell variations.

Moreover, the initial *ageing rate* does not allow any conclusions to be drawn about the potential occurrence of a knee point or the time of its event. Although a cell might degrade at a low or moderate speed at the beginning of its service life, a knee point can occur earlier than for a cell showing a higher initial *ageing rate*; compare the blue and red graphs in Figure 1. Furthermore, a knee point does not necessarily have to occur in the period under consideration, as the orange graph in Figure 1 indicates.

2.2. Definition of Accelerated Characterisation

Accelerated testing aims at reducing the test duration for ageing characterisation without altering the results for lifetime prediction under unaccelerated conditions. Therefore, an ***unaccelerated reference*** scenario needs to be defined with respect to the degradation progress and the necessary test time. With respect to automotive applications, it is common to use a daily or weekly driving pattern as a reference case,[32–36] as it reasonably reflects driving habits. These tend to include primarily short trips and thus low DoD with long resting periods of several hours to several days in between, as shown from mobility data analysis.[37] Consequently, the vehicle and, hence, the battery is idling most of the time. This means that the test duration would correspond to the service life to be demonstrated, which is generally set to 15 to 20 years.[2,3,38,39] Within the given time frames for application development of around 36 months[4] and the rapid technological progress,[5] this is not a viable approach.[24]

As described in the Introduction, we differentiate between two main approaches to achieve the desired accelerated characterisation and, thus, the reduction in test time: high precision measurements HPM and accelerated ageing methods AAM. The former intends to shorten the test time by increasing the measurement accuracy to detect *ageing mechanisms* at an early stage[40] which are not observable with ordinary equipment. The measured ageing behaviour is then extrapolated based on a dedicated model.[41] Consequently, the physical experiment can be terminated prematurely compared to the unaccelerated reference test. In contrast, AAM strives to amplify the *ageing mechanisms* that occur and thus accelerate the ageing progress without manipulating the ageing behaviour. For this purpose, intermediate idle periods are omitted, and/or *stress factors* are intensified by, e.g. elevated currents or temperatures, as will be discussed in the following sections. Commonly, only one *stress factor* is varied at a time to isolate its impact on ageing behaviour. Subsequently, combining several *stress factors* at the same time could maximise the acceleration of ageing.

As a fundamental prerequisite, lifetime prediction based on experimental data always requires, implicitly or explicitly, a ***model conception***. Hence, ageing not only has to be tested, but also has to be modelled to infer from a short-term experiment to long-term ageing behaviour.

2.3. Limits of Acceleration

One of the most important considerations is how much the ageing characterisation can be accelerated without altering the results for lifetime prediction. This is true for both HPM and AAM, although the limitations differ. In this context, it must be noted that we refer only to common operating conditions in this work. Extreme scenarios and abuse tests are not taken into account.

The HPM, on the one hand, is limited in terms of data accuracy. It is necessary that all occurring effects are detectable within the measurement data and that the model is able to extrapolate those effects adequately. On the other hand, it is limited to the minimum test duration required to provide enough data for lifetime extrapolation. In this regard, a crucial issue refers to determining the time at which sufficient data is accessible to appropriately parameterise the chosen model and hence reliably predict ageing. Both aspects are equally serious challenges with respect to the strong non-linearity of the ageing behaviour.

In contrast, the major challenge of AAM is to exactly amplify the *ageing mechanisms* that occur during the *unaccelerated reference* case without altering causality or causing additional ones. Consequently, limits arise beyond which the ageing behaviour changes, and ***consistency*** with the reference is no longer maintained. This means that, for example, under accelerated testing conditions, an initial linear *ageing trend* becomes progressive, as the dominating *ageing mechanism* switches and, therefore, might cause a knee point. Identifying those acceleration limits poses a massive challenge due to the highly complex cell behaviour and the partially non-linear cell characteristics, especially under manifold load conditions. Furthermore, those limits will not be valid across the board, but will depend heavily on the cell chemistry, properties, and manufacturer. Acceleration trends and limits are identifiable for individual groups of cells, such as specific cell chemistries or high-power and high-energy cell topologies, when comprehensive experimental ageing studies are conducted and carefully evaluated.[42,43]

In addition to the difficulty of ensuring *consistency* in the *ageing mechanisms* for the AAM method, as well as the high requirements on data quality for the HPM method, the challenge of ***transferability*** to the *real unaccelerated application* arises with both methods of accelerated ageing characterisation. This aspect addresses the question of how to translate the estimated battery lifetime from a laboratory test set-up into a real-world service life prognosis, for instance, the application-related mileage of electric vehicles.[44,45] For these reasons, ageing cannot be accelerated indefinitely, and therefore *stress factors* cannot be increased indefinitely. Therefore, in the next section, optimal accelerated testing strategies will be discussed.

2.4. Optimum in Accelerated Characterisation

Accelerated ageing tests aim to find an optimal compromise between shortening the test duration while preserving the *consistency* and *transferability* of the test results. The optimal acceleration points, which combine these two aspects, can be identified with extensive test matrices to investigate the *stress factor* related trends of ageing acceleration, but they are strongly linked to the cell chemistry and cell characteristics.

For example, several studies[23,24,39,46,47] have discussed the option of test acceleration by increasing charge and discharge current rates (C-rates) and thus reaching a specified number of cycles in a shorter period without altering the main occurring *ageing mechanisms*. They showed that the degradation modes are insensitive to the increased C-rates and therefore match the

unaccelerated reference. On the contrary, for real-world applications, the optimal operating conditions are where the lowest *ageing effects* occur. Hence, while accelerated ageing tests aim for the highest consistent ageing rate, the objective of optimal operational conditions in some real-world applications is the longest possible service life and, thus, the lowest possible ageing rate.

2.5. Disruptive Effects

During ageing tests, some effects need specific consideration, as they hinder a straightforward interpretation of HPM and AAM measurement data. In some way or another, they lead to an apparent capacity loss. Apparent capacity refers to the capacity loss that is measured during the test. However, this might differ from the irreversible capacity fade, which is of interest for characterising ageing if it includes a share of reversible capacity reduction. So we need to distinguish between the apparent capacity, including reversible effects, and the real capacity. Such effects that impact the ageing characterisation include the anode overhang effect and the path dependency. They will be discussed in the following.

Anode overhang effect. Ageing results can be significantly impaired by the anode overhang effect, which can distort the capacity measurement.

The anode overhang is defined as the excess anode area compared to the cathode area.[48–51] The anode is designed to be larger to allow alignment tolerance during production and to avoid lithium plating at the edges of the anode electrode. Additionally, if present, the double-coated anode that has no counter-cathode on the inner or outer parts of the cell adds up to the anode overhang. Therefore, lateral lithium ion transport takes place mainly through the electrolyte and is composed of diffusion due to concentration differences and migration due to lateral voltage difference in the anode.[49,52] The anode overhang effect has its root cause in longer time constants of this ion diffusion and migration compared to those of the charge and discharge cycles. This means that the anode overhang is (dis)charged with a time delay which might not be captured during capacity measurement.

To understand the effect, one has to consider the state of charge (SoC) before the test, which is typically around 20–30% due to delivery restrictions following UN3480. In case of a lower SoC during the ageing test, the active anode is charged by lithium ions flowing from the anode overhang, leading to capacity trends exceeding 100% or reducing irreversible losses.[48,49,53] In case of a higher SoC during testing than at delivery, the anode overhang reduces the extractable capacity as lithium ions flow to the anode overhang. At low temperatures, the diffusion coefficients are reduced, causing this effect to take several months to reach completion. A similar duration is needed at higher SoCs as a result of the flat anode potential curve, which leads to small voltage differences between the active anode and the anode overhang. In contrast, at higher temperatures and low SoCs, a few hours can be sufficient to reach equilibrium.[49] The anode overhang effect is fully reversible, cannot be deactivated[53,54] and applies to all cell chemistries with unequal electrode areas.

The anode overhang effect is most relevant at the beginning of the test and if the SoC or average SoC is changed during testing.[53] For full cycles, for example, the average SoC is 50% and therefore higher than the delivery SoC. In this case, the anode overhang effect must be considered only once in the beginning.[54–56] In contrast, when performing shallow cycles with different average SoCs or when the test includes rest periods at another SoC, the anode overhang effect will be triggered and therefore this effect must be considered throughout the experiment.[57] An example is given by Käbitz et al.[53] shown in Figure 2, where the capacity increases when switching to a lower average SoC (green) and decreases when switching to a higher average SoC (red). Beyond that, Gyenes et al.[58] reported the same phenomena by means of coulombic efficiency and visual inspections during post mortem analysis (PMA).

Even though the quality of production nowadays is significantly better, including low tolerance and intermittent coating, anode overhang still significantly disturbs ageing tests, especially accelerated ones. For tests with a low ageing rate, it may be of the same order of magnitude as irreversible losses. In the literature, this effect is often not considered and results must be read carefully as conclusions might be misleading. Similarly, a cathode overhang effect was observed for cells comprising an LTO anode.[59] The share of silicon in a composite with graphite will mainly influence the anode voltage curve and, with this, the speed of equalisation currents. The cathode materials have no significant influence on the effect.

To account for this effect during an ageing test, the maximum error due to this effect can be estimated by quantifying the excess anode area via cell disassembly or CT measurements. This is usually up to a few (2-5) percentage points of the nominal capacity. The smaller the cell, the larger the anode overhang in relation to the cell size. Alternatively, the introduction of a model is recommended. For equivalent circuit modelling, the anode overhang can be approximated as a capacitor with a long time constant depending on temper-

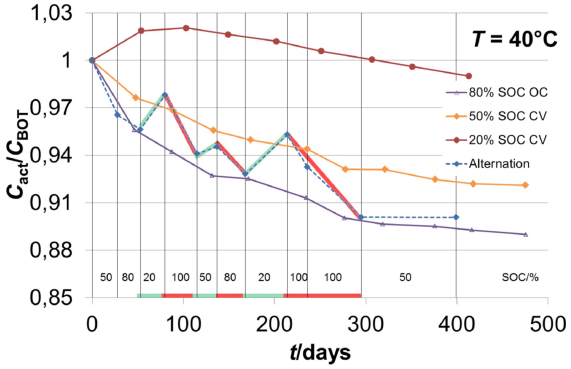

Figure 2. Beside static calendar ageing tests at 20%, 50% and 80% SoC, this figure provides the curve in dashed blue varying the SoC. To highlight the positive effect of a change to a lower SoC (green) and the negative effect of a higher SoC (red). Reproduced from Käbitz et al.[53] with the permission of Elsevier, 2023.

ature, voltage difference, and size of the anode overhang. For physicochemical models, one has to model not only a volume element but also the entire morphology of the winding or stacking. Promising model approaches are given by Azzam et al.,[52] Hildenbrand et al.,[60] Hüfner et al.[50] and Fath et al.[61]

For a relative comparison regarding the influence of, for example, the current rate in a defined DoD window, the anode overhang effect will contribute in a comparable way and the relative change will exclude the anode overhang effect.

Finally, the anode overhang effect must be considered and cannot be avoided after manufacturing. Its magnitude is only defined by the SoC before and during the test, while the speed is a function of the temperature and the difference in anode potential. To avoid negative influences on testing, we recommend performing tests without interruptions at random SoCs and waiting until the anode overhang effect is equilibrated. In case of fast testing, the anode overhang effect must be modelled.

Path Dependency. In ageing studies of LIBs, calendar and cyclic ageing conditions are commonly investigated under isolated and constant ageing conditions. However, there is evidence that the usage of constant conditions during the whole test cannot adequately cover the diverse interactions of different ageing conditions.[8,62] Instead, it is likely that there is a path dependency that describes ageing patterns that are not commutative. The history of the cell then has an influence on the ongoing ageing mechanisms and ageing effects. Under cyclic ageing conditions, path-dependent ageing was observed, e.g. for continuous cycling conditions.[63,64] In contrast, for temperature, there are examples in which path dependency was not observed in calendar ageing experiments.[65,66] Ageing tests with drive cycles close to the application may induce a more realistic combination of stress factors and lead to different results for ageing. Even if path-dependent ageing is assumed from the *ageing effects*, observations might be solely related to a change in the corresponding ageing trajectory of the *stress factor* and do not show real path dependency in ageing.[67] It should be acknowledged that a simple superimposition of ageing effects will not always be valid. As path dependency in ageing is complex and not well understood, clear recommendations of action cannot be given. For detailed information on path dependency, the reader is referred to.[62,68]

3. Methods

Despite the need to obtain results quickly, the importance of a thorough and holistic ageing analysis cannot be emphasised enough. Doing so can lead to unexpected results, such as a common inactive material (PET tape) that harms the cell[69] and reveals the root causes of failure. In this section, methods are presented to characterise calendar and cyclic ageing. It starts with conventional *reference performance test (RPT)* measurements that highlight critical aspects that must be considered during testing. Then HPM and AAM are discussed, followed by invasive methods to complement ageing tests. Their ability to characterise ageing in a fast manner is discussed, respectively. The section concludes with the statistical perspective on modelling and predicting ageing behaviour.

3.1. Cell Characterisation

In order to draw solid conclusions about the ageing phenomena in LIBs, the use of standardised *RPTs* is of primary importance in the execution of ageing experiments. Therefore, we will subsequently discuss commonly examined characteristics within a *RPT* and the ability to predict ageing using extensive characterisation methods at BoL.

3.1.1. Cell Characterisation Over Ageing

The basic approach to ageing tests is to assess the SoH of a lithium-ion cell regularly during steadily progressive ageing. By performing an initial predefined *RPT*, information on the pristine cell is retrieved, and a reference is set for any future *ageing effects*. By performing a similar characterisation on a predefined time or on a number of EFCs, the occurring *ageing effects* are tracked. The repeated performance of *RPT* over ageing is applied for accelerated or unaccelerated ageing tests where the influence of a specific *stress factor* is investigated.

Previous work[12,70,71] already provides an in-depth review of non-invasive characterisation techniques. The most common methods performed during an *RPT* for a LIB consist of three main components:

- **Capacity Measurement**: A specific charge-discharge cycle within the defined voltage limits at typically nominal C-rate and temperature to obtain a reference capacity value, used to estimate the SoH.
- **Low-current Measurement**: A specific charge-discharge cycle at a very low C-rate (e.g., C/50) to obtain material-specific electrode characteristics under a near equilibrium state. This can also be used to track *degradation modes* using incremental capacity analysis (ICA) or differential voltage analysis (DVA).
- **Resistance Measurement**: Several direct current step pulses in charge and discharge direction and electrochemical impedance spectroscopy (EIS) measurements at different SoCs to obtain information on internal impedance parameters and power capability.

To obtain accurate information about occurring *ageing trends*, these three elements are essential and cannot be substituted for each other. However, some approaches use the voltage hysteresis between charge and discharge[72] or the average discharge voltage[73] as a proxy value for resistance rise, which is especially interesting for silicon-based LIBs.[74] The correlation between resistance rise and capacity fade is not universal[75] but was reported for specific *degradation modes*. At low ambient temperatures, the extremely shortened lifetime can be correlated with irreversible processes leading to a strong resistance increase.[76–78] For cycling of nickel-containing cathodes at high temperatures, the capacity fade can be correlated with resistance rise.[79]

During the ageing test, cycling or storage is usually interrupted to perform a *RPT*. These *RPTs* can also impact cell ageing and alter the conclusions obtained. Furthermore, the fact that each *RPT* itself can take a very long time increases the overall test duration and impedes the feasibility of accelerated testing procedures. Hence, for a more precise determination of the actual available capacity under a certain investigated *stress factor*, the frequency of these measurements must be chosen carefully. The main objective is to acquire sufficient data points throughout the progression of the ageing without unduly disturbing it.[80,81]

The comparability of the values obtained from a *RPT* must be ensured by fixing a single set of conditions regarding temperature, C-rate, voltage range and cell compression. Thus, it is not beneficial to completely omit characterisation measurements for time-saving reasons and only use the capacity during ageing cycles to evaluate the *ageing trend*. Although this would reduce measurement time, comparability and precision are not given, limiting the conclusions on *ageing effects*.

The manufacturer usually sets additional limitations on the parameters in the data sheet. Taking these limitations into account, the safety risks are minimised, and the reference values can be obtained. For a better comparison between different test series, it is recommended to adhere to close-to-standard values commonly used in the literature, such as 1C or C/3 at 25 °C for the capacity measurement.[71] However, since the C-rate is not universally comparable, the energy content must also be considered, especially when comparing high energy and high power cells.[82]

Furthermore, the duration of a *RPT* is determined by the C-rates and the number of current pulses and pauses investigated. Hence, the most time-intensive step in a characterisation test is the low-current measurement. Therefore, finding the optimal compromise between time intensity and the significance of the lowcurrent measurement is important when designing characterisation routines. To do so, different low-current measurements in an initial characterisation test can be performed and analysed regarding the electrochemical information contained.

The reduction in the duration and frequency of the characterisation tests might not only lead to faster degradation analysis and data reduction, but also result in a more precise determination of the real available capacity under a certain investigated combination of *stress factors*.

In addition to the electrochemical characterisation during *RPTs*, thickness and pressure changes can serve as SoH indicators. The irreversible thickness increase of the anode can be linked to SEI growth and its lithium content.[83,84] This corresponds to the cell thickness if the cathode shows only minor changes in thickness. In contrast, Samad et al.[85] did not find a linear correlation of force with capacity fade but used the derivative of force with respect to charge similar to ICA as a health indicator. Mohtat et al.[86] measured the change in cell thickness under constant pressure within a cycle and cumulatively during cyclic ageing.

Although the irreversible expansion did not show a simple correlation with the capacity fade, the correlation of the maximum reversible expansion with capacity fade is linear for all of their tested ageing conditions. Because this expansion is mainly due to the graphite expansion in the anode, the reversible thickness change can be used as a reliable health indicator as long as the loss of active material on the anode is the dominant ageing mode.

While the thickness or pressure measurement during ageing tests requires a special test rig, thickness measurement before and after testing can be easily and inexpensively performed with a calliper. Therefore, the authors recommend including this simple method in every test.

3.1.2. Predictive Cell Characterisation

The *RPT* performed after production at BoL allows a detailed investigation that can be used to assess initial cell quality,[87] quantify cell-to-cell variations,[88,89] detect changes in cell design,[90] and identify damaged cells to discard them from further testing. This results in a more consistent ageing behaviour due to a lower initial variance.[91] Typical components to be assessed for cells already produced are open-circuit voltage, capacity, weight, and resistance.[92] In addition, non-invasive imaging can be performed to detect defects and production deviations. Examples are acoustic scanning imaging[93] or computed tomography.[87,94] The main feature of these methods is the short time required to provide insights.

In the initial characterisation, the starting values of quantities relevant to the *degradation modes*, such as usable anode capacity, usable cathode capacity and initial electrode balancing, can be quantified by ICA and DVA using half-cell measurements.[28,95] Already at BoL, this allows identifying the potential for hidden *ageing effects* such as loss of lithium inventory (LLI) compensation by an increasing delithiation of the silicon anode material,[96] cathode degradation hidden to the overall capacity[97,98] or marginal ageing before triggering severe ageing, such as lithium plating and consequential rollover.[9] Weng et al.[99] showed that some of the parameters mentioned above can already be extracted from the formation data before starting an extensive ageing test.

Another important electrochemical metric for ageing prediction is the rate capacity, in which the capacity at varying C-rate is measured.[100] The rate capability indicates the capacity sensitivity of a given cell design to a change in C-rate. A reduction in capacity translates into an increase in C-rate in an ageing scenario with fixed current or power. Thus, a low capacity decrease for increasing C-rates is an indicator of the robustness to cyclic ageing.[101] As the capacity is always measured in a fixed voltage window, the rate capability is directly linked to a cell's impedance.

An advanced method to measure cell resistance or complex impedance is EIS.[102] EIS holds the potential for ageing predictions in LIBs as it provides detailed information on the ohmic resistances and reaction kinetics of cells and, in some cases, the identification of the contribution of the anode and cathode.[103] As SoC and the temperature tremendously affect the impedance of the cell,[104] they must be chosen and

controlled carefully during the measurement. EIS has shown to be a powerful tool for predicting differences in ageing behaviour in groups of cells that seem to be identical by other metrics, for example, 1 kHz impedance or nominal/measured capacity.[92,105,106] It has also been used in electrochemical design studies to measure the impact of electrolyte compositions on degradation[40,72,107] or particle size distribution.[108] The impedance measurement can even be related to the cell balancing, as shown by Weng et al.[109]

The electrical data obtained during the formation of LIBs provides an insight into the electrochemical process of solid electrolyte interphase (SEI) formation, more precisely the reaction of the electrolyte components at the beginning of the first charge, which can be quantified by the peaks in ICA.[107] Quantifying the prevalence of certain reduction reactions allows us to understand the impact of design parameters such as electrolyte composition[107,110,111] on battery degradation. For further prediction of the impact of cell design parameters and formation protocols on battery degradation, coulombic efficiency and self-discharge rate are well established metrics.[40]

3.2. High Precision Measurement Techniques

In this section, HPM techniques are presented where *stress factors* are not increased with respect to the *unaccelerated reference*. Thus, the ageing itself is not accelerated. Instead, the acceleration in ageing characterisation is achieved merely by measuring with high precision, which makes side reactions detectable.

During ageing, parasitic side reactions occur that are not part of the main reactions of reversible lithium exchange between anode and cathode. In the following, we will clarify the term parasitic reactions, referring to reversible and irreversible shares, and discuss two promising HPM methods to assess the ageing of LIBs. The investigated methods are float current analysis (FCA) for calendar ageing and high precision coulometry (HPC) for cyclic ageing, both based on a highprecision current measurement.

3.2.1. Float Current Analysis

The float current analysis (FCA) is a method to determine calendar ageing with a self-discharge experiment that measures the current to keep the voltage constant.[48] Self-discharge is generally the voltage decay over time in idle mode.[112,113] The root causes of this decay can be mainly attributed to the slow redistribution of lithium ions over the electrode area, such as the anode overhang effect,[58,60,114] to reversible shuttle reactions leading to reversible loss of stored energy[115] or to irreversible side reactions, i. e. ageing.[116]

In FCA, the voltage drop during self-discharge is converted into a recharge current to keep the voltage constant. The results of the open-circuit voltage and constant voltage methods can be converted to each other using the dV/dQ value at the respective voltage and temperature.[117] After an initial transient period of constant voltage, both methods are equal for lower SoCs and temperature where the voltage decay over time is low and the recharge current is not expected to trigger additional reactions.[53,115,117] The measurement of voltage decay is more straightforward compared to the FCA. However, the evaluation is more challenging as the dV/dQ value changes, on the one hand, with temperature and SoC and, on the other hand, with ageing. This becomes significant especially when the voltage slope at the test SoC is very high, as is at the end of discharge or the end of charge, especially for LFP cathodes.

In the following, we consider only moderate ageing conditions concerning temperature and cell voltage, as are expected for cells with a service life of more than ten years. The measurement consists mainly of three phases as depicted by Azzam et al.[52] in Figure 3. After a transient phase of about one month in total at 30 °C, including less than one day for polarisation (1) and up to 30 days for the positive (b) or negative (a) anode overhang effect (2), the float current of the cell finally reaches steady-state (3). Thereby, it is reported[48,118] that the steady-state current shows a high correlation with the capacity loss rate (Figure 4a). The origin of the capacity loss was determined by evaluating the peak distances of anode and cathode in dV/dQ, revealing mainly LLI and not loss of active material (LAM). As the formation of SEI leads to LLI, the steady-state current corresponds to the loss rate (slope: Ah/h) in the representation of the remaining capacity over time. It increases with higher cell voltage and temperature and follows the Arrhenius law as exemplarily shown in Figure 4b.[48,118]

However, Schulze et al.[119] showed only a relative correlation for LFP/graphite cells with comparable trends and proposed that SEI losses due to voltage slippery could only be measured

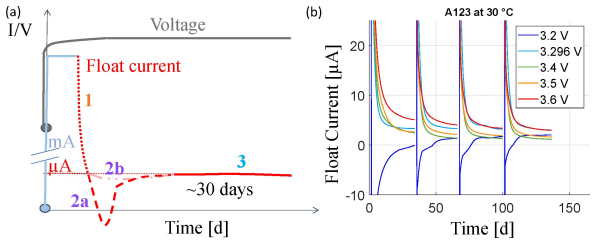

Figure 3. (a) Three phases of float current analysis with (1) polarisation, (2a) negative or (2b) positive anode overhang effect and (3) steady-state. (b) An example of 30 days of floating for five voltages at 30 °C for a lithium iron phosphate (LFP)/graphite cell. The graphic is reprinted from Azzam et al.[52] under Creative Commons Attribution 4.0 license, CC BY.

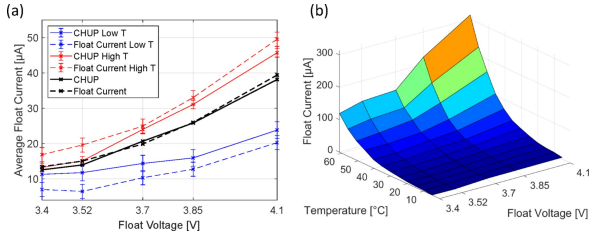

Figure 4. (a) Correlation results from capacity loss rate (RPT) and float currents for a low, high and combined temperature profile. (b) 3D plot for five voltages varied with temperature. The graphic is reprinted from Theiler et al.[118] under Creative Commons Attribution 4.0 license, CC BY.

to a high extent if the slope of the anode voltage is significantly greater than the slope of the cathode voltage curve. Lewerenz et al.[48] observed a strong counterexample where LFP/graphite cells were held at 100% SoC. In this experiment, a reasonably high current was measured. However, in this case, hardly any recharge current is expected, as the voltage slope is high for the cathode and negligible for the anode where delithiation occurs due to SEI growth.

Jagfeld et al.[120] demonstrated that the float current and capacity loss increase with a higher active surface of the electrodes, leading to higher float currents for high-power cells compared to high-energy cell types. Thus, for calendar ageing and float currents, the active surface and not the cell capacity is relevant and scale, therefore, not directly with nominal capacity.

As ageing occurs on one electrode while the entire battery is recharged, Azzam et al.[121] derived a scaling factor from the ratio of the voltage slopes of the anode to the full cell. It links the resulting float current to the ageing of the anode and the cathode, respectively. The authors could assign mainly anode sidereactions from SEI growth to float currents at lower SoCs and mainly cathode side-reactions to float currents at higher SoCs where the anode potential is flat. The cathode ageing can most likely be attributed to cathode lithiation caused by the decomposition of the electrolyte at the cathode leading to an increase in internal resistance.[122] While SEI growth reduces LLI, cathode lithiation would increase LLI and with this mask LLI caused by SEI growth. This could explain the highest ageing rate at about 80% SoC as reported, for example, by Rumberg et al.[123]

Thus, float currents represent cathodic and anodic effects that could influence LLI positively and/or negatively. More research is needed to assess the ageing and link the ageing with the capacity loss rate and the specific electrodes.

In addition to the active materials, cells contain passive materials that may lead to side reactions. For example, in cells containing a PET tape that secures the jelly roll, a strong shuttle-reaction was observed that significantly increases the float current and disturbs the analysis.[124] Therefore, float currents must be doublechecked for potential reversible contributions before assigning the float currents solely to ageing.

The reversible and irreversible nature of float currents can be further assessed by performing a capacity test before and after the floating experiment. As the discharge cut-off voltage is defined solely by the anode and the charge cut-off voltage by the cathode, one can assess the cathode, anode or coupled-side-reactions using the end-point-slippage method. This can be used for float currents.[117,125] Therefore, RPT tests before and after floating are recommended once anode overhang effect is equilibrated.

Assuming that the steady-state float current correlates with ageing and the capacity loss rate, a fast characterisation can be achieved by changing the temperature step-wise as shown in Figure 4b for NCA/NMC vs. graphite/Si.

While the conventional ageing tests with regular RPT measurements are influenced and distorted by the transient part at every measurement point due to cycling and the anode overhang effect,[48] FCA is influenced by transient parts only once in the beginning after the RPT before the float measurement.[52] This leads to a higher measurement and prediction precision, especially at the beginning of the test. Further, compared to the conventionally used RPT-based method with a sampling rate of typically 2 to 4 weeks at a reference temperature, FCA assesses irreversible losses continuously and directly at the test temperature, avoiding additional ageing effects due to cycles during the RPT.

Theiler et al.[118] showed for their investigated 2–3 Ah 18650 cells that the float currents are in the order of 1 to 10 μA at 10 °C and rise to about 100 to 300 μA at 60 °C depending on the cell voltage (3–4.2 V). Therefore, especially for smaller cell sizes, lower temperatures and SoC, high-precision equipment is necessary that provides stable voltage and current over temperature changes of the cells and the test device. Due to this temperature-induced noise at the device and the cell, filtering of the float current data becomes necessary and cannot be simply averaged.

The increase in internal resistance does not show a significant impact on the float currents, as Theiler et al.[118] demonstrated. A higher resistance leads only once to a higher overpotential, while the voltage decay is measured continuously. As the currents are sufficiently low, the overpotential resulting from increased resistance is negligible compared to the continuous voltage decay. Information about resistance over ageing, however, can be obtained before and after the FCA experiment in a RPT[114,118] and during the FCA using EIS at the test voltage and the reference or test temperature. Data for EIS at the test SoC combined with float currents have not yet been published. EIS is beneficial as it allows the measurement of the relative resistance change over time without changing the SoC. However, comparing the float tests with EIS, obtained not under reference conditions but at different SoCs and temperatures, is challenging, as the EIS measurements reveal strong dependencies on temperature and SoC. Thus, comparing the results of different test conditions is more complicated and has to be supported by a model.

For accelerated calendar ageing prediction, float currents are a promising candidate for accelerated calendar ageing prediction, especially for SoCs and temperatures close to an application with a long battery life-time. However, a quantitative correlation with capacity loss rate and SEI formation and potentially cathode lithiation remains to be proven and requires separating reversible and irreversible contributions to the float current. Moreover, high measurement precision is necessary, as slight deviations will lead to significant differences during extrapolation. The duration until steady-state is reached depends on the test SoC in the order of up to 30 days due to the anode overhang effect for float voltages above 4 V. An appropriate model could achieve a prediction of the steady-state before it is finally reached. This limitation will become negligible for smaller anode overhangs due to better manufacturing processes. Thus, lifetime predictions should be possible within weeks, but the literature has not yet proven this. Moreover, FCA can help to find *sweet spots* with constant

steady-state currents considering the stability of cells with respect to the combination of voltage and temperature.

3.2.2. High Precision Coulometry

Coulometry is an essential analytical technique in electrochemistry that quantifies faradaic reactions by measuring the total electric charge per cycle. With high precision coulometry (HPC), capacity loss is quantitatively and precisely measured over the first 20–30 cycles (3–4 weeks) without any rest periods and then extrapolated over the lifetime to assess the ageing behaviour.[126]

In modern cells, with typically long lifetimes, the capacity loss during a testing time of some weeks is very low. Therefore, a very high measurement precision is necessary. For example, cells with cycle numbers greater than 1000 EFC before reaching 80% remaining capacity exhibit a charge loss over one cycle (C/20) that is only $<0.03\,\%$.[126] Thus, the precision of coulomb counting must be better than 50 ppm to resolve the fourth decimal digit of the coulombic efficiency with one sigma accuracy. This is not achieved with standard but only with HPC test benches.

During HPC, the cells are cycled at a constant and low C-rate between set voltage boundaries that are typically the cut-off voltages but can also be any other predefined voltage. The effectiveness of the cell is then quantified by the coulombic efficiency, which is determined by the ratio between the discharge and the previous charge.[127]

Generally, the discharge capacity Q_d is lower than the charge capacity Q_c. Assuming only parasitic side reactions, the irreversible capacity loss per cycle is directly related to the lithium consumed in the side reactions. As the cells are cycled at low current rates, lithium loss is mainly caused by SEI growth[127,128] but can also be related to loss of electric or ionic contact of lithiated particles or lithium plating as a result of high cut-off voltage or poor cell balancing.

For uniform cell behaviour, it is imperative to establish a thermally stable environment, especially when the voltage endpoints are reached, as temperature significantly influences the overpotential and, therefore, the measurement of charge/discharge capacity.[126,129] Current measurement errors comprise parts of the absolute and full-scale values. For utmost precision, it is essential to use constant currents that are close to the full scale values of the measuring device.[126,127,130] Thus, dynamic profiles are, so far, beyond the scope of HPC.

For an accurate interpretation of the coulombic efficiency, the influence of the anode overhang (see Section 2.5) should be considered. Gyenes et al.[58] showed that at the beginning of the test, both an increase and a decrease in the coulombic efficiency are observable (Figure 5), which they related to the anode overhang effect. As depicted in Figure 5, all values are higher than unity for the first 20 days, and it took 75 days to reach a steady-state where active and passive anode have the same SoC.

As low C-rates are used for HPC, the change in overpotential is minimal, but the duration per cycle is comparably long and,

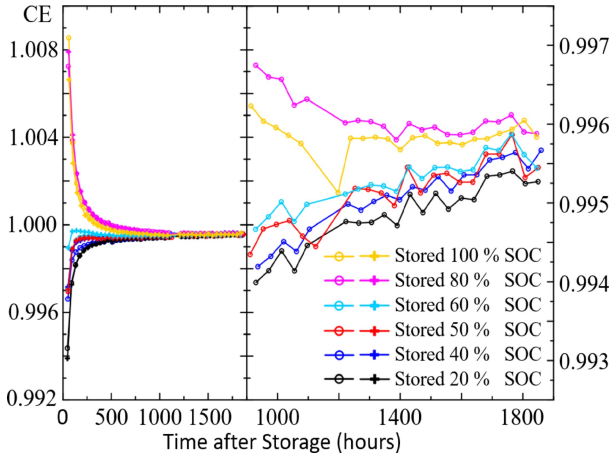

Figure 5. Coulombic efficiency of aged lithium nickel manganese cobalt oxides (NMC) pouch cells after 300 hours of open circuit storage at various SoC at 40 °C. The left panel shows full-scale data and the right panel shows a zoomed-in view for the last 800 hours. The graphic is reproduced from Gyenes et al.[58] under Creative Commons Attribution 4.0 license, CC BY.

with this, the time for side reactions to occur. Thus, applying a higher C-rate of C/10[127,131–133] compared to, e.g. C/20[40,58,72,107,127,128,132,134] may also lead to a higher coulombic efficiency, as there is less time for side reactions. Burns et al.[132] found that doubling the C-rate from C/20 to C/10 reduced the loss in coulombic efficiency by half. Smith et al.[127] revealed the same scaling with a reduction in the loss of coulombic efficiency by a factor of 2.4 when increasing the current from C/24 to C/10. Therefore, the duration of a cycle must be considered when evaluating and comparing results for different C-rates. A very low C-rate does not seem to improve the results, while the results are achieved faster with C/10 compared to C/20.

Due to the low currents, there is hardly any information on the impedance change during ageing. Therefore, HPC is further enhanced by adding EIS measurements. Burns et al.[40] observed that for two cells with different electrolyte additives and similar coulombic efficiency, the one with half the charge transfer resistance had a cycle life five times longer. This indicates that coulombic efficiency alone is insufficient to predict cell lifetime. However, by combining both methods, the authors improved the lifetime prediction. With one impedance measurement in advance, they ranked the remaining lifetime of the investigated cells based on their coulombic efficiency.

Due to the high precision in HPC, another method called *end point slippage* is reported in the literature.[135] This method can attribute side reactions to the individual electrodes. Therefore, the coulomb counting must be measured continuously for several full cycles, and the shifts at the end of charge and discharge are tracked. An illustration is shown in Figure 6. The shift on the left side ΔD is called discharge endpoint slippage, and on the right side ΔC is named charge endpoint slippage. Discharge endpoint slippage refers to side reactions at the anode that consume active lithium, like SEI growth or lithium plating. In contrast, charge endpoint slippage is assigned to side reactions at the cathode, such as electrolyte oxidation that

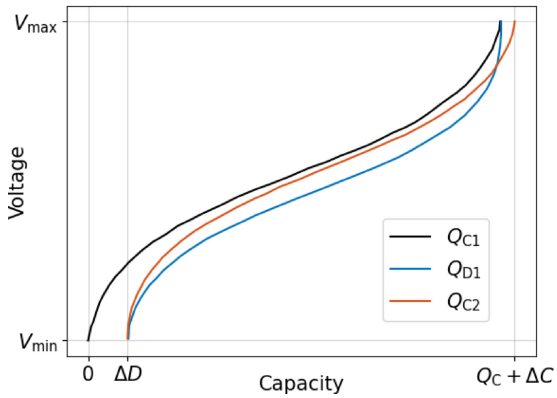

Figure 6. An illustration depicting the discharge endpoint slippage and charge endpoint slippage of a lithium-ion cell. Reproduced from Smith et al.[134] with the permission of IOP Publishing.

leads to additional active lithium in the electrode at the cost of $LiPF_6$ decomposition and increased resistance. If both effects co-occur, coupled side reactions are present between the anode and cathode.[115,136] The separation of charge and discharge endpoint slippage is valid only if the anode slope defines the discharge cut-off voltage and the cathode slope determines the charge cut-off voltage. This is generally the case for standard cell types and full cycles. Similar results for leakage capacities can be obtained for voltage hold and voltage decay measurements, suggesting that these methods are comparable in determining the amount of side reactions.[115] HPC and endpoint slippage assessment are also valuable for confirming similar amounts of side reactions taking place.[115] The study also indicates that endpoint slippage evaluation may not be able to quantitatively predict calendar ageing trends, as leakage capacity recorded during the hold may overestimate the irreversible capacity loss, and direct extrapolation of these methods may have limitations.[115] This implies that while HPC and endpoint slippage can provide insight into degradation mechanisms, their direct extrapolation may have limitations and caution must be exercised when using these methods to predict long-term battery lifetime.

Further, isothermal microcalorimetry, which measures the heat flow of parasitic side reactions, can enhance the early ageing characterisation. Higher parasitic heat flow can be correlated with lower coulombic efficiency and charge end point slippage, as well as to impedance increase and capacity fade.[116,137–140] Eldesoky et al.[140] could even attribute the measured heat flow to the reactions that occurred on the individual electrodes. Thus, isothermal microcalorimetry has the potential to make predictions about battery lifetime, especially when combined with HPC.

Overall, HPC is a suitable electrochemical method for studying *degradation modes* in batteries. Detecting subtle effects in modern, highly efficient cells requires a thermally stable environment, precise charge measurement, and clearly defined initial conditions. Coulombic efficiency provides information about the ageing mechanisms at low C-rates within 3–4 weeks. Comparing the coulombic efficiency of different cells enables a qualitative prognosis of their lifetime. In combination with impedance measurement, these predictions can be improved. For an understanding of anodic and cathodic side reactions as well as reversible charge losses, the evaluation of the endpoint slippages is suitable. Furthermore, HPC can be used in a RPT-based test design for evaluating the coulombic efficiency. Then, the precise measurement is performed only in RPT while during the ageing phase, *stress factors* are increased.

3.3. Accelerated Ageing Methods

During calendar and cyclic ageing tests, different *stress factors* can be applied to trigger particular *ageing mechanisms* and accelerate cell ageing in a desired way. For a detailed discussion of *ageing mechanisms*, their potential interaction and relation to *stress factors* the reader is kindly referred to other review articles.[7–11] In this section, we discuss the *stress factors* SoC, temperature, C-rates, and tests without rests for calendar and cyclic ageing tests and how they can be used to accelerate ageing characterisation with AAM. In this context, acceleration compares to an application scenario in which the battery is operated at an average SoC of around 50% with an average DoD of 50%, a temperature of 25 °C and moderate C-rates, including many rest periods.

For each stress factor, we provide a table at the end of this section summarising the ageing trends obtained in the literature. It gives the cell properties and testing conditions during ageing, the investigated stress factor, and how its increase influences the ageing rate. This shows whether the impact of the stress factor of interest on ageing behaviour is consistent across the literature.

3.3.1. State of Charge

The SoC refers to the amount of capacity stored in a LIB relative to a predetermined reference capacity; usually the nominal capacity.[141] It is directly related to the degree of lithiation and, thus, the potential of the electrodes. Therefore, the (average) SoC level will influence calendar ageing as well as cyclic ageing behaviour.

In general, for graphite-based LIBs, the observable *ageing rate* during calendar ageing is accelerated with increasing SoCs, which is consistent with the observed behaviour in the literature, as Table 2 shows. However, we must note that occasionally the highest ageing rate is measured at 80% SoC, as reported by Rumberg et al.[123] As it is not feasible to continuously utilise LIBs at low SoCs, a trade-off must be found between minimising accelerated *ageing effects* and ensuring feasible operating conditions.

On the cathode side, particularly electrodes composed of layered oxides contribute to the *ageing effects*. They display increased degradation for storage at high cathode potential, starting at a cell SoC of about 80%, especially in combination with high temperatures.[142] The reported *ageing mechanisms* are oxygen release,[143] electrolyte reaction,[142] transition metal

Table 2. Ageing trends reported in the literature for increasing the **storage SoC** in calendar ageing tests while temperature T was constant for all tests. The arrows ↗ and ↘ indicate a faster and slower degradation with increasing SoC, respectively, while for → the change in the ageing trend is inconclusive for the given conditions.

Reference	Chemistry	Form factor	Cap in Ah	n	T in °C	Rest at	Testing time in days	SoC in %	Change in ageing rate
Ecker.2012[170]	NMC-C	pouch	6	3	50 (35, 65)	OC/ CV	500	20, 50, 80, 100	→
Käbitz.2013[53]	NMC-C	pouch	10	2–3	40, 60	OC/ CV	400	20, 50, 80, 90, 100	↗ → (for 50–80 %)
Hoog.2017[32]	NMC-C	pouch	20	3	(25), 35, (45)	N/A	600	20, 35, 50, 65, 80, 100	↗
Gasper.2023[43]]	NMC-C	pouch	75	1	45, (55)	OC	230–290	20, 50, 80, 100	↗
Ecker.2014[219]	NMC-C	18650	2.05	3	50	CV	400	0, 10, 20, 30, 50, 60, 70, 80, 85, 90, 95, 100	↗
Keil.2016[156]	NMC-C	18650	2.05	1	25, 40, (50)	OC	300	0, 5, 10, 20, 30,	↗ (25 °C, 50–60 %)
								40, 45, 50, 55,	→ (25 °C, rest)
								60, 65, 70, 80,	↗ (50 °C)
								90, 95, 100	
Smith.2021[45]	NMC-C	prism	50	1	(25), 45, (55)	N/A	325	10, 50, 90, 100	↗ (10–90 %) ↘ (90–100 %)
Lewerenz.2018[49]	NMC-C	prism	25	3–4	50	CV	400	9, 19, 42, 65, 80	↗
Belt.2011[228]	NMC/ LMO-C	18650	1.2	5–10	30	OC	290	30, 90	↗
Bank.2022[59]	NMC-LTO	pouch	10.6	1	60, 80	OC	125–275	5, 55, 95	↗
Keil.2016[156]	NCA-C	18650	2.8	1	25, 40, 50	OC	300	0, 5, 10, 20, 30,	↗ (25 °C, 60–70 %)
								40, 45, 50, 55,	→ (25 °C, rest)
								60, 65, 70, 80,	50 °C: ↗ (50 °C)
								90, 95, 100	
Wildfeuer.2023[152	NCA–Si/C	18650	2.5	1	50	OC	672	10, 20, 30, 40, 50, 55, 60, 65, 70, 75, 80, 85, 90, 95, 100	↗ (10–50 % and 70–85 %)
Keil.2016[156]	LFP-C	18650	1.1	1	25, 40, (50)	OC	300	0, 5, 10, 20, 30,	→ (25 °C, 0–40: 80–100 %
								40, 45, 50, 55,	→ (25 °C, rest)
								60, 65, 70, 80,	↗ 50 %
								90, 95, 100	
SarasketaZabala.2014[25]	LFP-C	26650	2.3	1	40, (50)	OC	600	30, 70, 90	↗
Schimpe.2017[182]	LFP-C	26650	3	1	10, 15, 25, 35, 45, 55		max. 234	0, 12.5, 25,	↗ (0–37.5: 62.5–87.5 %)
								37.5, 50, 62.5, 75, 87.5, 100	→ (rest)
Kassem.2012[229]	LFP-C	cylin	8	3	30, 45, 60		150–250	30, 65, 100	→ (30 °C) ↗ (45,60 °C)
Lewerenz.2017[114]	LFP-C	cylin	8	3	25, 40, 60		150–850	20, 50, 80, 100	→ (25 °C) ↗ (40, 60 °C)

Cap – Capacity; C – graphite; prism prismatic cell; cylin – cylindrical cell; n – number of cells tested at each condition; OC – open circuit; CV – constant voltage Conditions in brackets () mean that they were not tested in every combination.
Brackets () after the arrows give the range in which the ageing rate changes accordingly.

Table 3. Ageing trends reported in the literature for increasing the **average SoC** in cyclic ageing tests while temperature T, depth of discharge DoD and C-rate were constant for all tests. The arrows ↗ and ↘ indicate a faster and slower degradation with increasing SoC, respectively, while for → the change in the ageing trend is inconclusive for the given conditions.

Reference	Chemistry	Form factor	Cap in Ah	n	T in °C	C-rate ch/dch	DoD in %	Cycle number	Average SoC in %	Change in ageing rate
Hoog.2017[32]	NMC-C	pouch	20	3 or 8	35	0.3C/1C	20, (10, 50, 100)	800–1200 EFC	10, 35, 50, 65, 80	→
Gao.2018[230]	NMC-C	pouch	8	1	25	6C/6C	20	3000 EFC	10, 30, 50, 70, 90	capacity:↗ → for (30–70 %) resistance:→
Lewerenz.2018[281]	NMC-C	prism	25	1	25 °C	1C/1C, 3C/3C	6, 12	2500–4000 EFC	9, 19, 42, 65, 80	↘ (9–42 %) ↗ (42–80 %)
Smith.2017[45]	NMC-C	prism	50	1	45	0.33C/1C	40, (60, 80)	N/A	30, 50, 70	→
Zhu.2017[231]	NMC/NCA-C	18650	2.5	2–5	25	1C/1C	20, 40, 60	700 EFC	(25), 35, 45, 55, 65, (75)	↘ (up to 50 %) then ↗
Krikaldy.2022[164]	NMC–Si/C	21700	5	2–3	10, 25, 40	0.3C/1C	30, 100	800 EFC	15, 50	→
Gantenbein.2019[232]	NCA-C	18650	2.6	1	25	1C/4C	20	4000	15, 35, 55, 75, 85	↗ (up to 75 %) ↘ (for 75–80 %)
Zhang.2019[233]	NCA-C	18650	3	2	30	0.3C/1C	20	600–900	10, 50, 90	→
Mikheenkova.2023[162]	NCA–Si/C	21700	4.6	N/A	22, 45	0.3C/1C	50	800–2500 EFC	25, 75	↘
Chowdhury.2024[163]	NCA–Si/C	21700	4.6	N/A	25	03C/1C	10	2000–4000 EFC	10, 20, 30 40, 50, 60, 70, 80, 90	↘ (up to 50 %) ↗ (50–60 %) then →
Spingler.2020[168]	LFP-C	26650	2.86	N/A	40	1C/1C	10 (20)	10000 EFC	25, 40, 45, 50, 55, 60, 65, 70, 75	→

Cap – Capacity; C – graphite; prism – prismatic cell; cylin – cylindrical cell; EFC equivalent full cycle; n – number of cells tested at each condition The number of cycles is given either in full cycles (no unit) or in equivalent full cycles (EFC).
Conditions in brackets () mean that they were not tested in every combination.
Brackets () after the arrows give the range in which the ageing rate changes accordingly.

Table 4. Ageing trends reported in the literature for increasing the **DoD** in cyclic ageing tests while temperature T, average SoC and C-rate were constant for all tests. The arrows ↗ and ↘ indicate a faster and slower degradation with increasing DoD, respectively, while for → the change in the ageing trend is inconclusive for the given conditions.

Reference	Chemistry	Form factor	Cap in Ah	n	T in °C	C-rate ch/dch	Average SoC in %	Cycle number	DoD in %	Change in ageing rate
Käbitz.2013[53]	NMC-C	pouch	10	2–3	40	1C/1C	5, 50, 75, 95	N/A	10, 50, 100	↗
Hoog.2017[32]	NMC-C	pouch	20	3 or 8	(25), 35, (45)	0.3C/1C	(20, 35), 50, (65, 80)	800–1200 EFC	10, 20, 25, 50, 65, 80 100	↗ for DoD > 50%
Jiang.2019[157]	NMC-C	pouch	8	3	25	6C/6C	10, 30, 50 70, 90	3100-5000 EFC	20, 100	↗
Gauthier.2022[234]	NMC-C	pouch	0.25	2	40	C/10, C/5, C/3	12.5, 25, 37.5, 50, 65.5, 75, 87.5	3370	25, 50, 75, 100	↗
Ecker.2014[219]	NMC-C	18650	2.05	1–3	35	1C/1C	10, 25, 50, 75, 90, 95	500–3000 EFC	5, 10, 20, 50, 80, 100	↗
Schuster.2015[195]	NMC-C	18650	1.95	3	35	1.2C/1.2C	50	up to 1900 EFC	27, 73, 87	↗
Preger.2020[42]	NMC-C	18650	3	≥2	15, 25, 35	0.5C/0.5C, 0.5C/1C, 0.5C/2C, 0.5C/3C	50	400–2100 EFC	20, 60, 100	↗
Lewerenz.2018[218]	NMC-C	prism	25	1	25 °C	1C/1C 3C/3C	9, 19, 42, 65, 80	2500–4000 EFC	6, 12	↗
Smith.2021[45]	NMC-C	prism	50	1	(25), 45	0.33C/1C	30, 50, 60, 70	N/A	20, 40, 60, 80, 100	↗
Zhu.2021[231]	NMC/ NCA-C	18650	2.5	2–5	25	1C/1C	(25), 35, 45, 55, 65, (75)	700 EFC	20, 40, 60	→
Bank.2020[235]	NMC-LTO	pouch	10.6	1	40	5C/5C	55 (50 for 100% DoD)	8000–12000 EFC	2, 5, 10, 20, 70, 100	→ (2–20%) ↗ (70–100%)
Wikner.2021 cite Wikner.2021	LMO/ NMC-C	pouch	26	1–2	25, 35, 45	2C/2C, 1C/2C	45, 50, 55, 85	1500–3000	10, 80, 90	↗
Zhang.2019[233]	NCA-C	18650	3	2	30	0.3C/1C	50	600–900	20, 50, 100	↗
Preger.2020[42]	NCA-C	18650	3.2	≥2	15, 25, 35	0.5C/0.5C, 0.5C/1C, 0.5C/2C	50	250–1600 EFC	20, 60, 100	↗
Wildfeuer.2024[152]	NCA–Si/C	18650	2.5	1	5	0.5C/2C	50	700–1500 EFC	20, 40, 60, 80, 100	↗
Preger.2020[42]	LFP-C	18650	1.1	≥2	15, 25, 35	0.5C/0.5C, 0.5C/1C, 0.5C/2C, 05C/3C	50	1600–3000 EFC	20, 60, 100	→
Wang.2011[180]	LFP-C	26650	2.2	2	(−30, 0, 15, 25, 45), 60	0.5C/0.5C	45, 60, 75, 90, 95	1-54943	10, 20, 50, 80, 90	→
Naumann.2020[169]	LFP-C	26650	2.85	3	40	1C/1C	25, 50, 75	2000-14000 EFC	1, 5, 20, 40, 80	→
Spingler.2020[168]	LFP-C	26650	2.85	N/A	40	1C/1C	50	10000 EFC	5, 10, 20, 40, 60, 80, 100	↗ long-term

Table 4. continued

Reference	Chemistry	Form factor	Cap in Ah	n	T in °C	C-rate ch/dch	Average SoC in %	Cycle number	DoD in %	Change in ageing rate
Lewerenz.2017[114]	LFP-C	cylin	8	3	40	1C/1C	50	3000–8000 EFC	10, 50, 100	↑

Cap – Capacity; C – graphite; prism – prismatic cell; cylin – cylindrical cell; EFC – equivalent full cycle; n – number of cells tested at each condition The number of cycles is given either in full cycles (no unit) or in equivalent full cycles (EFC).
Conditions in brackets () mean that they were not tested in every combination.
Brackets () after the arrows give the range in which the ageing rate changes accordingly.

dissolution,[144,145] and transformation of the crystalline structure.[145,146]

On the other hand, the graphite anode has a low electrode potential, which makes it thermodynamically unstable within most common organic liquid electrolytes.[147] This results in electrolyte reduction and lithium oxidation, forming an SEI that serves as a protective passivation layer.[148] Increasing the cell SoC lowers the graphite potential even further in a stage-wise manner with constant voltage plateaus in each stage.[149] Hence, higher storage SoCs increase the amount of intercalated lithium within the graphite structure. During calendar ageing, this intercalated lithium reacts with electrolyte solvents diffused through the SEI, leading to gas formation and thickening of the SEI layer.[150,151]

The addition of silicon in the anode does not fundamentally change the observed calendar ageing behaviour compared to pure graphite anodes.[152] Cells comprising an LTO anode exhibit very little degradation.[59]

The observed *ageing trend* during calendar ageing is widely described as square root behaviour over time, with the fastest capacity fade occurring during the first weeks of storage based on the theoretical growth of SEI.[153,154]

However, Attia et al.[155] challenge the unquestioned use of the $t^{0.5}$ dependency, as it often overestimates ageing at the beginning while underestimating it in the long term. This inaccurate estimation can be mainly attributed to the omission of the anode overhang effect, as described in 2.5, which greatly influences the measured capacity in the initial ageing stage. In particular, when cells are stored at very high or very low SoCs, an initial steep decrease or increase in capacity becomes visible, which can be considered reversible.

The results of Käbitz et al.,[53] indicate that cells stored at SoCs within the same graphite voltage plateau display a similar *ageing trend*, whereas SoCs at lower voltage plateaus led to stronger *ageing effects*. The results of Keil et al.[156] show a similar ageing behaviour, in which cells stored at SoCs above 60% experienced an abrupt increase in ageing. However, the initially dominating anode overhang effect potentially strongly influences this behaviour.

Figure 7a depicts the *ageing trend* for a calendar-aged cell stored at 20% SoC, respectively 80% SoC extracted from Käbitz et al.[53] The cell stored at a low SoC of 20% exhibited an initial increase in capacity, followed by an inflection point, after which the capacity decreases linearly. In contrast, the cell stored at 80% SoC initially experienced a sharp decrease in capacity, followed by a more gradual linear trend. This is explained by the anode overhang effect, initially the primary effect influencing capacity, leading to a sharp increase in capacity for the cell stored at 20% SoC and a rapid capacity decrease for the cell stored at 80% SoC. As a result, an initial offset appears in the capacity fading gradient, leading to an inflection point that indicates the subsequent dominance of the *ageing trend* by SEI growth.

Hence, neglecting the anode overhang effect leads to a misinterpretation of the SoC dependence for calendar ageing, as the initial reversible offset must be differentiated from irreversible ageing, especially at high and low SoCs. Taking into

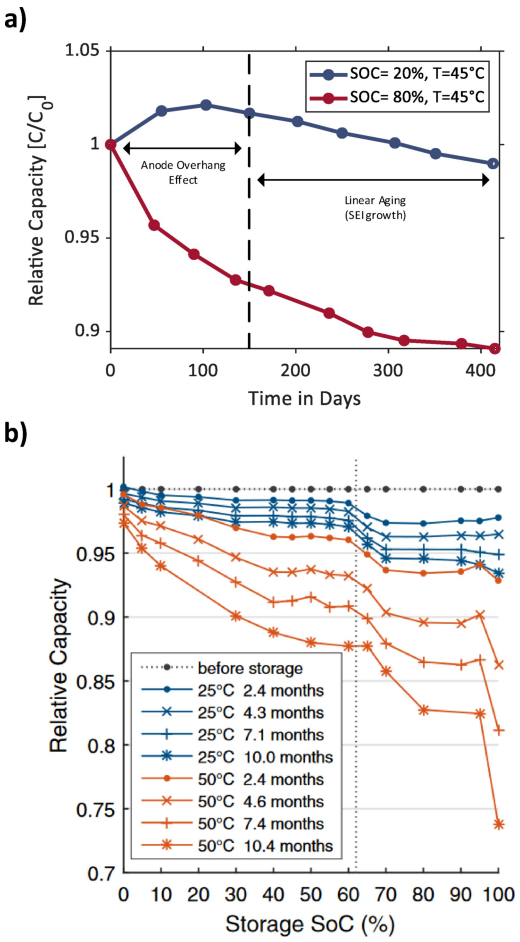

Figure 7. a) Capacity loss trajectory for cells stored at 20% SoC and 80% SoC (Reproduced from Käbitz et al.[53] with permission of Elsevier, 2023) b) Calendar ageing for an NMC cell at different SoCs, indicating strong initial offset due to the anode overhang effect. (Reproduced from Keil et al.[156] under Creative Commons Attribution 4.0 license, CC BY)

account the dominant anode overhang effect, especially in the initial ageing stage, leads to the conclusion that a linear *ageing trend* might predict the irreversible long-term ageing behaviour during calendar ageing more precisely.

Figure 7b depicts the capacity fade for calendar-aged cells at various storage SoCs and 25 °C ambient temperature, extracted from Keil et al.[156] Comparing the initial capacity before storage with the initial capacity loss observed after 2.4 months reveals a notable difference. Especially for cells stored above 60% SoC, the initial capacity loss is considerably more distinguished than for cells stored below 60% SoC. However, considering the subsequent capacity fading rate, it becomes evident that the ageing rate decreases significantly, particularly for cells stored above 60% SoC. This again indicates that the initial more considerable discrepancy in capacity, primarily stemming from the anode overhang effect, strongly influences the early ageing stages as an offset. In contrast, the subsequent irreversible ageing is less eye-catching.

Hence, the *sweet spot* of the *stress factor* SoC for accelerated calendar ageing is found to be between 60% 90%. On the contrary, accelerated cathode degradation is expected for cells stored at 100% SoC,[45] thus altering the overall ageing behaviour. However, depending on the amount of excess graphite active material, higher full cell storage SoCs can be utilised without reaching the SoC regime of highest capacity fade, which highlights the importance of evaluating initial battery characteristics, as mentioned in Section 3.1.1. Additionally, more accurate predictions on irreversible ageing effects are possible considering the anode overhang effect and delivery SoC.

Despite the increase in ageing with increasing SoC during calendar ageing tests, continuous cycling within high and low SoC windows leads to faster capacity fade. In contrast, for around 50% SoC, the lowest loss was reported in various publications (cp. 3). Hence, during cyclic ageing, the utilised SoC window appears to impact the occurring *ageing effects* immensely. For example, Jiang et al.[157] found that cells cycled with 100% DoD exhibited almost twice the capacity loss of cells cycled with low DoD (20% around 50% mean SoC) for an equal charge throughput. This effect was attributed to a higher volume expansion during full cycles and more severe graphite degradation.[158]

More precisely, the host materials undergo crystallographic transformation as a function of their lithiation, which is associated with increased particle strain and particle cracking.[159,160] The volume expansion of the anode materials leads to pronounced SEI cracking, restoring contact between the lithiated graphite and the electrolyte. This again results in more severe SEI growth and is accompanied by LLI and LAM on the negative electrode.[23,161]

The effect of volume expansion is especially true for negative electrodes containing silicon. Silicon exhibits a volume expansion of up to 300% and is active at low full cell SoC. Thus, cells cycled in low SoC regions suffer from a high loss of active material on the anode.[162,163] This effect explains the different ageing trend for silicon-containing cells in Table 3. As the capacity loss of silicon highly dominates the overall capacity fade,[164] a high average SoC is beneficial for the lifetime. The contradictory relations of materials with SoC need to be considered when designing the test matrix to capture the ageing behaviour comprehensively, as silicon degradation may not be observed if no measurements are conducted in low-average SoC.[152]

At the cathode, LAM on the positive electrode is especially prominent during cycling at high SoCs.[165,166] In addition to LAM, cycling at high SoCs leads to the dissolution of transition metals and hence further accelerates SEI growth.[7,167]

However, for LiFePO4/graphite cells, an opposing correlation was found, as shallow cycling around 50% mean SoC led to greater degradation due to the flat cathode voltage curve and the voltage hysteresis of LiFePO4.[114,168]

Cycling within high SoC regions generally accelerates degradation. However, this trend is not consistent throughout the SoC range and for all results presented in the literature, as Table 3 shows. Additionally, the DoD has an impact on the ageing rate (cp. Table 4). In general, a higher DoD leads to a higher capacity fade, which is more pronounced for NMC and NCA cells than for LFP.[42] However, the impact of SoC on cyclic

ageing is strongly correlated with other *stress factors*, which will be discussed in more detail in the following sections.

It should be mentioned that the effect of increased calendar ageing at high SoCs is always superimposed while performing cyclic ageing tests. Hence, ageing models become necessary, which aim to calculate the pure cyclic *ageing effects*.[36,169,170]

3.3.2. Temperature

The environmental temperature condition in which a battery is operated depends on the application and climate. However, the internal temperature and the temperature distribution are relevant for the cells' ageing behaviour. This is determined not only by external conditions but also by the cell-specific internal heat generation and heat transport pathways toward the thermal environment. External conditions thereby incorporate the ambient temperature as well as the design and operating strategy of a thermal management system, if present. In contrast, internal heat generation depends on electrical current and resistance as a function of SoC, SoH and temperature and is affected by the chemistry and design of the cell. In the following, the potential of temperature as a *stress factor* to accelerate ageing is shown, first for calendar and then for cyclic ageing, as well as the limits at which different *ageing mechanisms* start to occur.

Calendar ageing is the simplest test case and shows high reproducibility. The effect that increasing temperature accelerates ageing is consistent in the literature, as Table 5 shows. Several publications demonstrated the validity of the law of Arrhenius for both capacity fade and resistance increase, indicating an exponential relationship between temperature and reaction rates.[65,170,171] That means that all *ageing mechanisms* related to parasitic side reactions and therefore ageing itself are accelerated at higher temperatures. The most dominant *ageing mechanisms* during calendar ageing are SEI growth at the anode and, if combined with a high SoC, the transition metal dissolution and electrolyte decomposition at the cathode.

This Arrhenius dependency of cell ageing on temperature suggests the highest ageing rate at the highest possible temperature. However, Lewerenz et al.,[114] for example, found a massive spread in results at a testing temperature of 60 °C for cells that showed good reproducibility under normal operating conditions. This increase in variation is one hint that a limit has been exceeded and ageing is not accelerated in a desired manner.

Besides accelerating the occurring *ageing mechanisms*, additional ones are triggered if the temperature exceeds a certain

Table 5. Ageing trends reported in the literature for increasing the **temperature** in calendar ageing tests while the SoC was constant for all tests. The arrows ↗ and ↘ indicate a faster and slower degradation with increasing temperature, respectively, while for → the change in the ageing trend is inconclusive for the given conditions.

Reference	Chemistry	Form factor	Cap in Ah	n	SoC in %	Testing time in days	T in °C	Change in ageing rate
Ecker.2012[170]	NMC-C	pouch	6	3	50, 100 (20, 80)	500	(25), 35, 50, 65	↗
Käbitz.2013[53]	NMC-C	pouch	10	2–3	50, (100)	400	25, 40, 50, 60	↗
Hoog.2017[32]	NMC-C	pouch	20	3	20, 35, 50, 65, 80, 100	500	25, 35, 45	↗
Ecker.2014[219]	NMC-C	18650	2.05	1–3	50	400	35, 40, 50	↗
Lewerenz.2018[49]	NMC-C	prism	25	3–4	42	400	30, 40, 50	↗
Smith.2021[45]	NMC-C	prism	50	1	30, 50, 60, 70	201–300	10, 25, 45, 55, 60	↘ (10–25 °C) → (25–45 °C) ↗ (45 °C–60)
Belt.2011[228]	NMC/LMO-C	18650	1.2	5–10	60	320	30, 40, 50, 60	↗
Werner.2021[65]	NCA-C	pouch	3	2	(20, 90) 35, 50, 65, 80, 100	max. 700	40, 50, 60	↗
Waldmann.2015b[204]	NCA-C	18650	3.25	1	50	N/A	6, 23, 40, 60	↘ (6–25 °C) → (above 25 °C)
Wildfeuer.2023[152]	NCA–Si/C	18650	2.5	1	10, 50, 70, 100	100–672	20, 35, 50, 60	↗
Schimpe.2017[182]	LFP-C	26650	3	1	0, 12.5, 25, 37.5, 50, 62.5, 75, 87, 5, 100	max. 234	10, 15, 25, 35, 45, 55	↗ (from 15)
Kassem.2012[229]	LFP-C	cylin	8	3	30, 65, 100	150–250	30, 45, 60	↗
Lewerenz.2017[114]	LFP-C	cylin	8	3	50, 100	150–850	25, 40, 60	↗
Gasper.2023[43]	LFP-C	prism	250	1	100	230–250	30, 45, 55	↗

Cap – Capacity; C – graphite; prism prismatic cell; cylin – cylindrical cell; n – number of cells tested at each condition
Conditions in brackets () mean that they were not tested in every combination.
Brackets () after the arrows give the range in which the ageing rate changes accordingly.

level. In cells containing the conductive salt lithium hexafluorophosphate ($LiPF_6$), for example, the SEI is thermally unstable at temperatures above 60 °C[17] and reacts with the electrolyte or active material.[172] Independent of temperature, LTO anodes do not exhibit significant degradation until 80 °C.[59]

Looking solely at the individual components, the upper temperature limit of $LiPF_6$ salt is 70 °C and the upper temperature limit for typical carbonate-based electrolyte components is between 90 °C and 120 °C before they start to decompose.[16] This is in the range of the onset temperature for thermal runaway.[173] Thus, in this case, ageing is clearly inconsistent with the *unaccelerated reference* and even poses safety risks. Therefore, the maximum temperature for accelerated ageing characterisation should be slightly lower than the temperature at which thermal instabilities first occur but not higher to ensure *consistency* and *transferability*. However, this upper temperature limit depends on the exact composition of the cell. With more stable electrolytes, such as those using LiTFSI salts, good cycling performance is achieved even at 100 °C. The capacity fade follows the Arrhenius dependency and lifetime is not limited by decomposition reactions, but by the permeation of electrolytes through pouch seals.[174]

The lower temperature limit with respect to ageing and stability is defined by the melting point of the electrolyte, which is, e.g. at −25 °C for the binary EC/DMC (3:7) with 1 M $LiPF_6$.[175]

Considering cyclic ageing, the Arrhenius law for parasitic side reactions is still valid. However, it has to be taken into account that heat is generated during operation, so that the internal cell temperature is higher than the surface temperature. Both reversible entropic heat generation and irreversible Joule heating contribute to this effect. The latter is increasing and becoming more dominant with a higher C-rate. Depending on the kind of temperature control and operating conditions, there is the risk of underestimating the internal cell temperature and exceeding – at least in some regions – the maximum temperature at which further *ageing mechanisms* are triggered. For high C-rates and large cells, more than 10 K internal temperature differences can arise.[176]

Diao et al.[24] recommend 60 °C for accelerated ageing tests as capacity fade and impedance increase were highest at those temperatures for their LCO/graphite pouch cells. The empirical model they developed could capture the ageing behaviour for different temperatures. However, they did not verify the ageing conditions for consistent ageing mechanisms. Gao et al.[46] investigated the dominant *ageing mode* responsible for the knee-point. They found LAM at the anode decreasing with increasing temperature while LAM at the NMC cathode became more dominant with rising temperatures until 45 °C. However, they did not test at temperatures higher than 45 °C and therefore did not specify a maximum temperature for acceleration.

Tan et al.[177] found consistent ageing mechanisms for their LFP cells even at 60 °C.

Jalkanen et al.[178] cycled 40 Ah pouch cells at room temperature, 45 °C, and 45 °C/65 °C, respectively. Postmortem analysis showed that the increased resistance and capacity fade with higher temperature result from alterations of the graphite anode, separator, and amount of residual electrolyte. These effects were stronger with increasing temperature. However, only for high-temperature cycling at 65 °C, the NMC cathode exhibited particle cracking and delamination. Thus, by triggering this additional *ageing mechanism*, the limit for accelerating ageing by increasing temperature was exceeded.

Agyei Appiah et al.[179] suggested using a physicochemical model to identify the maximum temperature for cycling LMO/graphite cells. Validated with cycling data, they found that the maximum temperature and, therefore, the optimum temperature for accelerating ageing is 45 °C. Until this temperature SEI growth is the most dominant ageing mechanism, while manganese dissolution becomes more dominant at elevated temperatures.

Besides the higher ageing rate at higher temperatures, cyclic ageing is also more severe at lower temperatures. Wang et al.,[180] for example, showed that a different *ageing mechanism* occurs when a cell is cycled at 0 °C compared to cycling at temperatures above 15 °C. This acceleration of ageing during charging is typically associated with lithium plating due to lower state diffusion coefficients and reaction rate constants.[17] An additional exponential function can describe this behaviour.[77,181,182] Superimposed with the Arrhenius law, this leaves an optimum temperature for cyclic ageing with accelerated ageing at both higher and lower temperatures, as visualised in Figure 8. The change in slope clearly marks a transition in ageing mechanisms.[176] However, this optimum temperature and ageing rates change with C-rate and state of health[183] as well as cell chemistry and designs.[42] Additionally, it was reported to be different for capacity fade and impedance increase.[184]

Table 6 shows that the effect of increasing temperature is consistent in the literature. However, there are a few studies in which the cells do not exactly exhibit the behaviour mentioned above. Instead, there are limited temperature ranges in which the temperature does not significantly affect the ageing rate.

Additional temperature effects need to be considered during cycling. Ruiz et al.[185] found different dependencies of

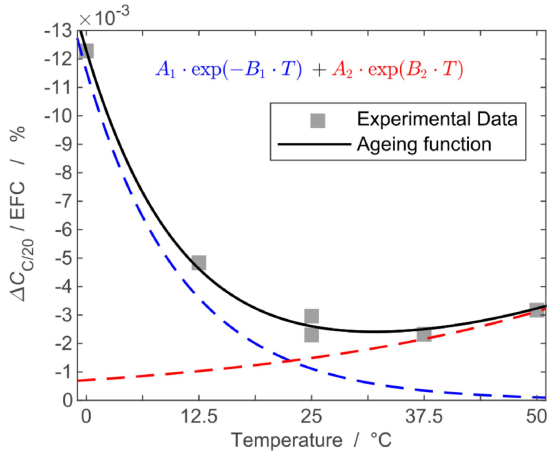

Figure 8. Ageing rate depending on temperature. The graphic is reprinted from Werner et al.[184] under Creative Commons Attribution 4.0 license, CC BY.

Review
doi.org/10.1002/batt.202300594

Chemistry Europe
European Chemical Societies Publishing

Table 6. Ageing trends reported in the literature for increasing the **temperature** in cyclic ageing tests while average SoC, depth of discharge DoD and C-rate were constant for all tests. The arrows ↗ and ↘ indicate a faster and slower degradation with increasing temperature, respectively, while for → the change in the ageing trend is inconclusive for the given conditions.

Reference	Chemistry	Form factor	Cap in Ah	n	C-rate ch/dch	DoD in %	Average SoC in %	Cycle number	T in °C	Change in ageing rate
Käbitz.2013[53]	NMC-C	pouch	10	2–3	1C/1C	10, 50, 100	5, 50, 75, 95, 100	/	25, 40, 60	↗
Jalkanen.2015[178]	NMC-C	pouch	40	1	1C/1C	100	50	1500–2500	room temperature, 45, 45/65	↗
Hoog.2017[32]	NMC-C	pouch	20	3 or 8	0.3C/1C	20, 35, 50, 65, 80, 100	50	800–1200 EFC	25, 35, 45, (50)	↗ (for DoD > 35)
Gao.2019[46]	NMC-C	pouch	36	2	1C/1C	100	50	500–900	25, 35, 45	→
Schuster.2015[195]	NMC-C	18650	1.95	3	0.5C/1C	94	50	600–1800	25, 35, 50	↘ (25–35 °C) ↗ (35–50 °C)
Preger.2020[42]	NMC-C	18650	3	≥2	05C/1C, 05C/2C	100	50	180–780 EFC	15, 25, 35	↘ (15–25 °C) ↗ (25–35 °C)
Epding.2019[81]	NMC-C	prism	25	1	1C/2C 2C/1C	100	50	300–900	10, 23	→ (1C/2C) ↗ (2C/1C)
Smith.2021[45]	NMC-C	prism	50	1	0.33C/1C	20, 40, 60, 80	30, 50, 60, 70		10, 25, 45, 55, 60	↘ (10–25 °C) → (25–45 °C) ↗ (45 °C–60)
Nemeth.2020[236]	NMC–C-LTO	pouch	10	1	10C/10C	100	50	4200-12000 EFC	25, 45	↗
Nemeth.2020[236]	LMO/LCO-LTO	prism	2.9	1	10C/10C	100	50	20000 EFC	25, 45	↗
Kirkaldy.2022[164]	NMC–Si/C	21700	5	2–3	3C/1C	100	50	~800 EFC	10, 25, 40	capacity: ↘ (10–25 °C) → (25–24 °C) resistance: ↗
Waldmann.2014[181]	NMC/LMO-C	18650	1.5	N/A	1C/1C	100	50	638	−20, −10, 0, 25, 50, 60, 70	↘ (−20–25 °C) ↗ (25–70 °C)
Werner.2020[184]	NCA/LCO-C	pouch	3	2	3C/3C	100	50	750–4500 EFC	0, 25, 50 (avg. T 12.5, 37.5)	↘ (0–25 °C) ↗ (25–50 °C)
Kucinskis.2022[183]	NCA/ LNO–Si/C	21700	5	2	0.2C/0.5C 0.4C/0.5C 0.6C/0.5C	100	50	max. 600	−15, −10, −5, 0, 5, 15, 25, 30, 35, 45, 50, 55, 60	↘ (−15–25 °C) ↗ (25–45 °C) slight change in optimum T with C-rate
Waldmann.2015[176]	NCA-C	18650	3.25	N/A	0.5C	100	50	50–250	0, 5, 15, 20, 25, 30, 40, 50, 60	↘ (0–25 °C) → (25–60 °C)
Preger.2020[42]	NCA-C	18650	3.2	≥2	0.5C/1C, 0.5C/2C	100	50	250–1500 EFC	15, 25, 35	↘ (15–25 °C) → (25–35 °C)
Diao.2019[24]	LCO-C	pouch	3.36	8	profile/ 0.7C profile/ 1C, profile/2C	100	50	100–750	10, 25, 45, 60	→ (10–25 °C) ↗ (25–60 °C)
Spitthoff.2023[237]	LCO-C	pouch	6.55	≥2	1C/1C, 2C/2C (3C/3C)	100	50	250–2000 EFC	5, 15, 25, 35, 45	capacity: ↘ (−5–15 °C)

Table 6. continued

Reference	Chemistry	Form factor	Cap in Ah	n	C-rate ch/dch	DoD in %	Average SoC in %	Cycle number	T in °C	Change in ageing rate
										↗ (25–45 °C) resistance: ↗
Leng.2015[238]	LCO-C	prism	1.35	1	0.5C/1C	100	50	250	25, 35, 45, 55	↗ (capcity and resistance)
Ruiz.2017[185]	LFP-C	pouch	6	2	1C/1C	100	50	~100	−20, −5, 5, 12, 30	↗ from −5–30 °C
Tan.2013[177]	LFP-C	18650	1.45	N/A	1C/1C	100	50	~250–550	25, 40, 50, 60	↗
Preger.2020[42]	LFP-C	18650	1.1	≥2	0.5C/1C, 0.5C/2C	100	50	2500–9000 EFC	15, 25, 35	↗
Wang.2011[180]	LFP-C	26650	2.2	2	0.5C/0.5C; 2C/2C, 2C/6C, 2C/10C	10, 20, 50, 80 90	95, 90, 75, 60 55	1-54943	−30, 0, 15, 25, 45, 60	↘ (0–60 °C)
Schimpe.2017[182]	LFP-C	26650	3	1	0.25C/ 0.25C, 0.5C/0.5C 1C/1C	100	50	1500–3000 EFC	0, 10, 25, 55	↘ (0–25 °C) ↗ (25–45 °C)
Gasper.2023[43]	LFP-C	prism	250	1	0.65C/ 0.65C	80	60	1500–2000 EFC	10, 30, 45	→

Cap – Capacity; C – graphite; prism – prismatic cell; EFC – equivalent full cycle; n – number of cells tested at each condition. The number of cycles is given either in full cycles (no unit) or in equivalent full cycles (EFC). Brackets () after the arrows give the range in which the ageing rate changes accordingly.

the ageing rate on the charging and discharging temperature for an LFP pouch cell. The charging temperature had a greater impact on the ageing than the discharging temperature. Furthermore, the temperature effects on the *ageing mechanisms* and *ageing effects* cannot be isolated, but must be considered interdependently with electrical current and SoC. Cycling at different temperatures, for example, results in varying overpotentials which are lower at higher temperatures. Hence, the same upper cut-off voltage is reached at a higher SoC, which increases the risk of particle cracking at the cathode as an additional *ageing mechanism*.[84]

Furthermore, other effects lead to additional *ageing mechanisms* and acceleration limitations. External temperature control combined with internal heat generation inevitably leads to an inhomogeneous temperature distribution and, therefore, to non-uniform *ageing mechanisms*.[186] If the temperature gradient parallels the electrode layers, the overall ageing roughly follows the respective average temperature,[77,184] while a gradient perpendicular to the layers leads to accelerated ageing.[187] For this scenario, Fleckenstein et al.[188] found by simulation that the ageing corresponds to an average internal cell temperature plus 10% of the maximum temperature difference.

Furthermore, Carter et al.[189] proved on coin cells that the directionality of a temperature gradient determines at which electrode *ageing mechanisms* are dominant. A temperature difference between the electrodes of only 2 K showed significant effects. Moreover, they showed that lithium plating occurs when the anode is slightly colder than the cathode, even at an average temperature of 35 °C and a current of C/5.

As mentioned above, plating is usually associated with low temperature and high charging current. Still, temperature transients during charging can trigger plating even at higher temperature levels.[84,190] This effect can be related to the inter-electrode temperature difference when the anode has a lower temperature than the cathode. However, these mechanisms are highly in homogeneous and have not yet been well understood.

Overall, temperature is – within certain limits and very few exceptions – a *stress factor* very well suited to accelerate the occurring *ageing mechanisms*. The acceleration follows exponential functions, which may have different pre-exponential coefficients and activation energies depending on the specific cell chemistry. The possibility of temperature gradients and transients should be considered during the test setup and data evaluation. Especially the interdependencies with electrical current, SoC, and heat generation have to be taken into account.

3.3.3. Current Rates

If the LIB is operated with sufficiently low current rates, the *ageing mechanisms* and *ageing effects* closely match the calendar ageing at the respective temperature and average SoC. This is especially true for high temperatures.[191] Then, time is the more relevant *ageing variable* compared to charge throughput. This changes gradually with higher C-rates.[169]

Thus, increasing the current rate has an accelerating momentum on the test duration. For cyclic ageing tests, the charge throughput is commonly used as *ageing variable*, and with an increased current rate, a higher charge throughput and, thus, a higher number of EFC can be reached in the same period of time.

For the acceleration of actual ageing, a higher C-rates increases the mechanical stress on the active materials. They are coupled with faster and more inhomogeneous volumetric changes as a result of the increased intercalation rate of lithium ions. This mechanical stress has been reported to cause fractures, cracks, and contact loss between particles in the electrode and binder, resulting in contact loss between particles and current collectors.[160,192,193] These processes lead to LAM and LLI. In addition, exposure of the cracked particle surface to the electrolyte leads to electrolyte decomposition[194] and active lithium consumption (LLI).[7,144] These factors have been reported to increase gradually with C-rates.

Consequently, in many studies, ageing was accelerated with increasing C-rates, as Table 7 shows. A lifetime performance investigation accelerated by increasing C-rates has been reported to return results comparable to the unaccelerated reference for lower C-rates ($<$1C).[195] However, transferable ageing in early stages does not exclude later ageing to be different, for example, due to an earlier onset of the rollover (knee point). As a potential limit, Sun et al.[192] have found for C-rates of 4C and higher, the dominant *ageing mechanism* changing from LLI due to SEI growth to structural decay of LFP and SEI. However, other studies did not find a clear ageing trend with increasing C-rates. Guan et al.[39] found an optimum C-rate of 1.8C for LCO by analysing the occurring *ageing mechanisms* in a post-mortem analysis.

Additionally, Schuster et al.[195] reported slower degradation with higher discharge currents. This is explained by reaching the end of discharge voltage earlier due to higher overpotentials, thus reducing the anode's mechanical stress. Keil et al.[196] obtained similar results with accelerated capacity fade and impedance increase for lower discharging rates.

Wang et al.[197] also observed a faster degradation when cycling at lower current rates. When the cells were opened, they found more lithium plating for lower currents. Higher currents entail higher ohmic losses in the cell, leading to a higher heating rate. At moderate or high temperatures, this leads to faster temperature-driven degradation (cp. Section 3.3.2.). In contrast, at low testing temperatures, the internal cell temperature increases into a region with lower degradation rates. Therefore, higher currents may even decelerate ageing and increase lifetime. Thus, the impact of higher Crates strongly depends on other *stress factors*, especially the test temperature. Barcellona et al.[198] tried to uncouple these effects and found the same ageing rate with respect to capacity for their tested discharge rates of 0.8C, 2.5C, and 5C.

High currents are also reported to foster an inhomogeneous lithium distribution, leading to high reversible capacity losses.[54,199] This must be considered to avoid attributing reversible ageing effects to actual ageing, as described in detail in Section 3.3.5 "Testing Without Resting".

Table 7. Ageing trends reported in the literature for increasing the **C-rate** in cyclic ageing tests while temperature T, depth of discharge DoD and average SoC were constant for all tests. The arrows ↗ and ↘ indicate a faster and slower degradation with increasing C-rate, respectively, while for → the change in the ageing trend is inconclusive for the given conditions.

Reference	Chemsitry	Form factor	Cap in Ah	n	T in °C	DoD in %	Average SoC in %	Cycle number	C-rate ch/dch	Change in ageing rate
Gao.2019[46]	NMC-C	pouch	36	2	25, 35, 45	100	50	500–900	1C/1C; 0,5C/1C; 1C/1,5C; 1C/2C	↗
Gauthier.2022[234]	NMC-C	pouch	0.25	2	20, 40	25, 50, 75, 100	12.5, 25, 37.5., 50, 65.6., 75, 87.5	3370	0.1C/0.1C, 0.2C/0.2C, 0.3C/0.3C	DoD: ↘ (75 and 100 %) → (25 and 50 %)
Schuster.2015[195]	NMC-C	18650	1.95	3	25, 35, 50	100	50	180–1900	0.5C/0.5C; 1C/0.5C; 0.5C/1C; 0.2C/0.5C; 0.5C/2C	charge: ↗ discharge: →
Keil.2019[196]	NMC-C	18650	2.05	≥ 3	25	100	50	278–957 EFC	0.7C/1C, 1C/1C, 1C/2C	charge: ↗ discharge: ↘
Preger.2020[42]	NMC-C	18650	3	≥ 2	15, 25, 35	20, 60, 100	50	400–2100 EFC	0.5C/0.5C, 0.5C/1C, 0.5C/2C, 0.5C/3C	discharge: ↘
Lewerenz.2018[218]	NMC-C	prism	25	1	25	6, 12	9, 19, 42, 65, 80	2500–4000 EFC	1C/1C, 3C/3C	↗
Epding.2019[18]	NMC-C	prism	25	1	10, 23	100	50	300–900	1C/2C, 2C/1C	↗
Wikner.2021[23]	NMC/LMO-C	pouch	26	1–2	25, 35, 40, 45	10, 80, 90	5, 15, 45, 50, 65, 85	1500–3000	1C/1C, 2C/2C, 4C/4C, 1C/2C	↗
Preger.2020[42]	NCA-C	18650	3.2	≥2	15, 25, 35	20, 60, 100	50	250–1600 EFC	0.5C/0.5C, 0.5C/1C, 0.5C/2C	discharge: ↘
Preger.2020[42]	LFP-C	18650	1.1	≥2	15, 25, 35	20, 60, 100	50	1600–3000 EFC	0.5C/0.5C, 0.5C/1C, 0.5C/2C, 0.5C/3C	discharge: → (up to 2C) ↗ (3C)
Dubarry.2014[239]	LFP-C	26650	2.6	N/A	N/A	100	50	350	0.5C/0.4C; 0.5C/0.2C; 0.5C/0.5C; 0.5C/1C	↗
Dubarry.2014[239]	LFP-C	26650	3.2	N/A	N/A	100	50	500	0.5C/0.4C; 0.5C/0.2C; 0.5C/0.5C; 0.5C/1C; 0.5C/2C	↗ (after ~200 dycles)
Schimpe.2017[182]	LFP-C	26650	3	1–3	0, 10, 25, 55	100	50	150–3000	0.25C/0.25C, 0.5C/0.5C, 1C/1C, 1.7C	→ (depends on T)
Naumann.2020[169]	LFP-C	26650	2.85	3	40	1, 5, 20, 40, 80	25, 50, 75	2000–14000	0.2C/0.2C, 0.5C/0.5C, 0.5C/1C, 1C/0.5C, 1C/2C	→
Lewerenz.2017[114]	LFP-C	cylin	8	3	40	50	50	2000-8000 EFC	1C/1C, 2C/2C, 4C/4C, 8C/8C	(1C-4C) ↗ (8C)
Sun.2018[192]	LFP-C	prism	0.58	N/A	25	100	50	500–3000	0.5C/0.5C, 0.5C/1C, 0.5C/2C, 0.5C/3C, 0.5C/4C, 0.5C/5C	↗
Barcellona.2020[198]	LCO-C	pouch	10	1	20–30	60	50	1500 EFC	0.8C/0.8C, 2.5C/2.5C, 5C/5C	→

Table 7. continued

Reference	Chemsitry	Form factor	Cap in Ah	n	T in °C	DoD in %	Average SoC in %	Cycle number	C-rate ch/dch	Change in ageing rate
Diao.2019[24]	LCO-C	pouch	3.36	8	10, 25, 45, 60	100	50	100–750	profile/0.7C profile/1C, profile/2C	→
Spitthoff.2023[237]	LCO-C	pouch	6.55	≥ 2	(5), 15, 25, 35, (45)	100	50	250–2000 EFC	1C/1C, 2C/2C, 3C/3C	capacity: ↘ (−5–15 °C) ↗ (25–45 °C) resistance: ↗

Cap – Capacity; C – graphite; prism – prismatic cell; cylin – cylindrical cell; EFC – equivalent full cycle; n number of cells tested at each condition The number of cycles is given either in full cycles (no unit) or in equivalent full cycles (EFC).

Furthermore, it has to be distinguished between the charge and discharge current as increasing the C-rate in charge direction increases the risk of lithium plating for graphite anodes. This is especially true for high SoC and low temperatures. It contributes to irreversible cell degradation by increasing LLI and the anode resistance. Hence, a detailed investigation of the propensity of plating to occur, as proposed by [81, 200] is reported to be a fast method to investigate lifetime performance, which allows isolating the single effect of current rates. Keil et al.[196] found a different dependency for discharging and charging rates, as higher charging rates led to a non-linear ageing trajectory. Similarly, Su et al.[47] found that the charging C-rate has a greater impact on *ageing effects* than the C-rate during discharge. Additionally, Attia et al.[201] found that SEI growth occurs mainly during lithiation of the carbon black in a half cell, which emphasises the asymmetry between charge and discharge. These findings are supported by modelling work.[202,203]

When evaluating the ageing acceleration with higher C-rates, these contradicting effects must be considered. Furthermore, not only the charging current, but also the charging strategy, has a tremendous impact on lifetime.[3,46,204] This shows again the close interaction of stress factors and the challenge of separating their effects on accelerated ageing.

3.3.4. Pressure

Mechanical compression of a cell affects many parameters like electrode distance, porosity, and tortuosity, which mainly change the dynamic parameters of a cell.[15] As the influence of pressure appears primarily in cyclic tests, but not in calendar ageing tests, there are no contributions to calendar ageing and mechanical pressure in the literature. This section focusses on findings for pouch cells with homogeneous pressure distribution to understand the underlying effects.

Lithium-ion pouch cells degrade significantly faster and perform worse if they are cycled fully uncompressed.[205–208] Thus, at least a certain compression in the range of 50–200 kPa improves performance and lifetime. The influence of pressure on performance and lifetime behaviour has been investigated in the literature. However, to the best of our knowledge, it has never been used as a stress factor to accelerate ageing tests. In this section, we discuss the optimal pressure conditions with respect to the initial offset pressure and the stiffness of the apparatus for accelerated cyclic ageing tests to achieve an optimal prognosis.

Contradicting ageing trends have been reported with increasing initial pressures, as summarised in Table 8. Li et al.[15] offer a review of various publications on the influence of external pressure during ageing and performance tests. Herein, an increment[209] and a decrement[210] of internal resistance were observed during performance tests with increasing initial pressure. Similarly, a faster,[205,208,211] as well as a slower[206] capacity fade was reported with increasing initial pressure. Both tendencies motivate the existence of an optimal initial pressure range for prolonging battery lifetime and the necessity of a

Table 8. Ageing trends reported in the literature for increasing the **initial pressure** in cyclic ageing tests of pouch cells and/or with higher **pressure change** during cycling due to cell breathing while temperature T, depth of discharge DoD, average SoC and C-rate were constant for all tests. The arrows ↗ and ↘ indicate a faster and slower degradation with increasing pressure or pressure change, respectively, while for→ the change in the ageing trend is inconclusive for the given conditions.

Reference	Chemistry	Cap in Ah	n	T in °C	DoD in %	Average SoC in %	C-rate ch/dch	Cycle number	Setup	Initial offset pressure in kPa	Change in ageing rate	Pressure change	Change in ageing rate
Barai.2017[206]	NMC-C	15	2	25	50	75	1C/1C	1200	rigid: plates and screws	0, 34, 103	↘	N/A, assumed high (rigid fixture)	–
Choi.2018[207]	NMC-C	35	1	40	80	55	profile	610 EFC	soft: springs	0, 20, 40	↘	0, 33, 68 kPa/mm 0, 61, 907 kPa/mm	↗ ↗
Wünsch.2019[208]	NMC-C	37	1	23	100	50	1C/1C	500–3000	rigid: plates and screws, soft: springs, silicone pad	0	–		↗ without pressure
Holland.2019[214]	NMC-C	5	1	RT	100	50	2C/2C	2000	rigid: plates and screws	40, 57, 97, 134, 182, 434	→	N/A, assumed high (rigid fixture)	–
Zhang.2020[211]	NMC-C	37	5	RT	100	50	0.5C/0.5C	3000	rigid: plates and screws, soft: springs, silicone pad	69	–	N/A, assumed low (springs), mid (pads), high (rigid fixture)	↗
Deich.2021[212]	NMC-C	60	1	25	100	50	step charge/1C	1000	controlled: hydraulic	16.7, 25, 45, 65, 73.3	↗	0.55, 3.2, 9.6, 16, 18.6 Mpa/mm	↗
Mohtat2021[86]	NMC-C	pouch	5	1–2	45	100	50	2C/2C	soft: springs	6.9, 34.5, 68.9, 103.4, 137.9, 172.4	↘ ↗	(6.9–103.4 kPa) (rest)	–
Lewerenz.2018[218]	NMC–C*	25	1	RT	6, 12	9, 19, 42, 65, 80	1C/1C, 3C/3C	4000	rigid: plates and screws	696	↗	222 kPa/1000DOD	↗
Cannarella.2014[205]	LCO-C	0.5	3	RT	100	50	0.5C/0.5C	800–2000	rigid: plates and screws	0, 50, 500, 5000	↗ (no pressure) → (50–500 kPa) ↗ (5000 kPa)	0, 500, 1000, 1500 kPa/100DOD	↗

C – graphite; prism – prismatic cell; EFC – equivalent full cycle; n number of cells tested at each condition, RT room temperature
The number of cycles is given either in full cycles (no unit) or in equivalent full cycles (EFC).
Brackets () after the arrows give the range in which the ageing rate changes accordingly. *prismatic cell

Chemistry Europe
European Chemical Societies Publishing

deeper understanding of additional aspects regarding pressure, like pressure distribution and pressure change during cycling.

Using more rigid apparatuses, i.e. higher pressure change due to cell breathing, leads unambiguously to a faster capacity loss.[205,207,208,211–213] Depending on the rigidity of the compression apparatus, the change in cell volume due to lithiation can induce pressures up to 1.6 MPa, even with an initial pressure of only a few kPa.[212] In studies using a rigid apparatus, a higher initial pressure will also increase the pressure change due to cycling.[205] Different elastic elements can be used to reduce the pressure change, such as battery pads or springs.[208,211] The higher pressure change correlates with the higher capacity loss during cycling in these experiments. Furthermore, Holland[214] used a controlled machine to ensure a target pressure despite cell breathing during cycling. All cycled cells had the same capacity loss rate despite initial pressures ranging between 40 and 400 kPa, challenging the findings of previous authors and motivating further research on the effects of the pressure change due to breathing. The impact of pressure change during continuous cycling will be discussed in the next section.

In summary, a certain initial pressure is considered positive. Higher initial pressures have inconclusive results, whereas higher stiffness of the apparatus is detrimental to lifetime and performance. Thus, we suggest using, where possible, a flexible setup with a pressure of 75 kPa for accelerated ageing tests. However, no reasonable pressure can be set externally in a hard casing as for cylindrical cells. In these cells, an uneven pressure distribution may result in heterogeneous degradation mechanisms.[215]

3.3.5. Testing Without Resting

For a typical long-life application, such as electric vehicles, batteries are typically used only 1–2 hours per day, resulting in a duty cycle of less than 10%. Additionally, charge and discharge current rates are on average less than C/5. To accelerate the characterisation of LIB, current rates are increased and resting periods are completely eliminated during testing. With this increase in the duty cycle to 100%, it is possible to achieve test results in a reasonable time frame.

In such AAM tests for hard-case (cylindrical) or externally fixed (pouch, prismatic) cells, a not yet discussed but very decisive effect on capacity fade was reported, which cannot be explained by the anode overhang effect.[48,49,58] It appears as an apparent capacity fade, which can be partly recovered by including test pauses. This effect is based on the assumption that high-current cycling leads to a successive increase in inhomogeneous charge and discharge over the elec trode area by local differences such as temperature, pressure, and porosity. Eliminating the rest phases results in less time for rehomogenisation of the lithium distribution within the electrode. Consequently, in an RPT, this inhomogeneous lithium distribution leads to a lower extractable capacity because the cutoff voltages are reached earlier during cell operation.

Several authors,[54,81,199,216] who added a rest period after cycling, found that cells regain capacity, as plotted exemplarily in Figure 9 (a). At the same time, the characteristic features of the DVA, which had flattened during cycling,[54,199,217,218] recovered strongly after a rest period, as shown exemplarily in Figure 9 (c). Moreover, they reported that this flattening is observed only for the anode features, while the cathode features did not change over cycling. Hence, inhomogeneous lithium distribution leads to a lower coherence of anode areas during charge and discharge, which can be visualised in the flattening of DVA features of the anode. Comparable results for visualisation of these inhomogeneities were found with an alternative method that evaluated the capacity difference of high and low currents. Authors observed a rise during cycling[216] and a decay during rest.[54,158,199,218] All of these findings suggest that for continuous cycling, an inhomogeneity in the lithium distribution over the anode area builds up that needs resting time to balance and finally reach an even lithium distribution.

Further, in shallow cycling experiments, the influence of this effect on the pressure change over breathing (dP/dSoC), called here pressure gradient, showed a strong impact on inhomogenisation. In the case of cycling in the lower and higher SoC ranges, where there are high pressure gradients, a more pronounced inhomogenisation of the areal lithium distribution was found. This is presented exemplarily as the interplay between apparent capacity loss and pressure gradient in Figures 9 (a) and (b). However, cycling around 50% average SoC where dP/dSoC is flat, the DVA does not indicate significant inhomogeneities.

Consequently, no recovery effect was observed, leading to the assumption that pressure gradients are the key origin of this reversible effect.[54,199] Remaining in high or low pressure gradient regions, Lewerenz et al.[54,218] investigated the dependence of the apparent capacity fade on the C-rates 1C and 3C and the DoD of 6% and 12%. Based on the flattening of the DVA features, they found a higher areal inhomogenisation with higher DoD and C-rate. Looking at the ageing rates over average SoC in Figure 10, this inhomogeneity leads to a

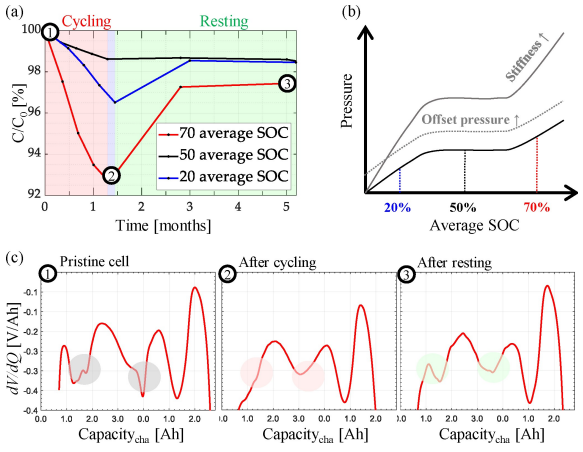

Figure 9. Interplay between (a) apparent capacity loss, (b) pressure gradient over SoC, and (c) inhomogenisation of lithium distribution during accelerated ageing (AAM) test of an NCA/graphite + silicon 18650 cell with resting phases. The graphic is modified from [199] under Creative Commons Attribution 4.0 license, CC BY.

Table 9. Brief overview of statistical tools and models in LIB testing.

Source	Ageing condition	Obj.	Modelling quantity	Dependencies	Sample size (tested cells/ tested conditions/ measurements per cell)	Method	Type of estimation & inferential approach
Ecker.2014[219]	calendar	1	capacity	voltage, temperature	73/20/4-9	linear regression on t	ordinary least squares
Schmid.2020[244]	calendar, cyclic	3	relative capacity	temperature	3/3/7–24, 13/3/7–13	linear regression on t	ordinary least squares, goodness of fit
Stroe.2014[278]	calendar, cyclic	1	capacity face, pulse power	temperature, cycle depth, SoC	3/3/13	linear regression on t non-linear system (4 parameters)	ordinary least squares
Käbitz.2013[53]	calendar	1	capacity fade	temperature, voltage	34/13/approx. 9–12	linear regression on t and $\sqrt{t}$	ordinary least squares
Gao.2019[46]	cyclic	3	SoC	temperature, C-rate	12/6/approx. 5–33	non-linear system (4 parameters)	non-linear least squares
Ecker.2012[170]	calendar	1	capacity fade	temperature, SoC	9/3/approx. 9	non-linear system (3–6 parameters)	non-linear least squares
Diao.2019[24]	cyclic	1, 2	capacity	temperature, discharge C-rate, charge cut-off, C-rate	196/24/approx. 3–16	non-linear system (7 parameters)	non-linear least squares
Werner.2021[65]	calendar	1	capacity	SoC, temperature	38/17/approx. 7–14	non-linear system (9 parameters)	non-linear least squares
Liu.2019[269]	cyclic	1,3	voltage, capacity loss	temperature, discharge C-rate	10/5/approx. 7	non-linear system (14 parameters), linear regression on PESA[a]	Bayesian MCMC[b], ordinary least squares
Baumhöfer.2014[88]	cyclic	1	lifetime	temperature, C-rate, voltage	48/1/1	linear regression (24 attributes)	ordinary least squares, cross validation
Johnen.2021[254]	cyclic	1	capacity	model assumes constant stress	48/1/13, 24/1/22	sigmoidal degradation with Gaussian errors	maximum likelihood inference, asymptotic, bootstrapping
Johnen.2020[267]	cyclic	1	lifetime	model assumes constant stress	48/1/1	parametric lifetime distribution (Weibull, lognormal, inverse Gaussian)	maximum likelihood inference, asymptotic inference
Harris.2017[265]	cyclic	1	lifetime	model assumes constant stress	24/1/22	parametric lifetime distribution (Weibull, normal)	maximum likelihood inference, median rank regression
Gewald.2020[252]	cyclic	2	capacity, resistance	temperature, discharge C-rate, SoC, DoD	16/16/2, 30/30/3	one-factor ANOVA[c]	F-statistic tests
Su.2016[47]	cyclic	2	capacity deceleration	C-rate, voltage, temperature, duration in CV stages	36/18/1	multi-factor ANOVA[c]	F-statistic tests
Xu.2019[248]	cyclic	1	capacity	rest time	4/1/approx. 134–168	linear Wiener process	maximum likelihood inference, online Bayesian
Richardson.2019[262]	cyclic	1	capacity difference	current, voltage, temperature	26/7/approx.10–43	Gaussian process regression, gradient boosting regression	maximum likelihood inference, kernel optimisation
Severson.2019[255]	cyclic	1	capacity	model assumes constant stress	124/1/150–2300	elastic net linear	maximum likelihood inference, cross validation, MCMC[b] sampling

Table 9. continued

Source	Ageing condition	Obj.	Modelling quantity	Dependencies	Sample size (tested cells/ tested conditions/ measurements per cell)	Method	Type of estimation & inferential approach
Long.2019[264]	cyclic	1	capacity	model assumes constant stress	1/1/168	neural network	back propagation,gradient descent

Objective (Obj.) coding: 1. Lifetime estimation and prediction; 2. Stress factors and their effect analysis; 3. Ageing mechanism identification [a] Positive Electrode Equivalent Active Surface Area; [b] Markov chain Monte Carlo; [c] Analysis of variance.

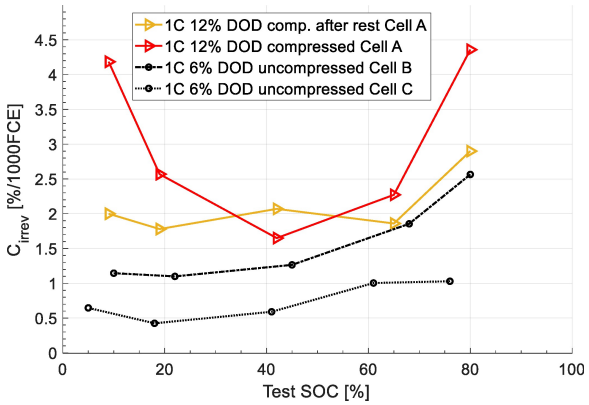

Figure 10. Capacity loss rate over average SoC during cycling for compressed (red), compressed after resting (orange)[54] and two different uncompressed (black) cells.[213].

v-shaped curve (red) based on [54,213,219]. However, after resting the cell (orange),[54] a successive increase in ageing rates over the average SoC is reported, which fits very well with the results for uncompressed pouch cells (black), underlining the contribution of pressure gradients.[53,213] The inhomogenisation of the lithium distribution acts as a precursor for lithium plating[220] and is, therefore, only reversible in an early stage of AAM testing.

In addition to the pressure gradient between different areas of the electrode, the voltage gradient over SoC is relevant for rehomogenisation. Despite the previous results based on layered oxide cathode materials, Spingler et al.[168] found the highest apparent capacity losses for LiFePO4-graphite cells when cycling around 50% average SoC. In this region, firstly, the hysteresis effect of LFP is strongest and secondly, on both electrodes the voltage over SoC is hardly changing. Thus, the inhomogeneities that developed during continuous cycling are not rehomogenised. This is supported by the work of Lewerenz et al.[114,221] who found higher capacity losses and lithium plating for cycling LFP cells between 45 and 55% average SoC. Thus, the recovery velocity is driven by the voltage difference of the inhomogenised electrode areas and is most likely hindered by their SoC-induced pressure difference.

Another effect related to inhomogeneities is reported for continuous cycling. During charging, the volume of the anode expands and pushes the electrolyte out of the pore volume into the excess void space of the cell.[222,223] During discharge or rest periods, the electrolyte moves back into the pore space. However, this process might take longer than the subsequent discharge, reducing the amount of electrolyte in some parts of the electrode. By omitting rests during the ageing test, this temporary electrolyte deficiency potentially causes inhomogeneous *ageing mechanisms*. To understand this effect and its implications, further research is necessary.

In summary, AAM, with continuous cycling as a stress factor combined with high currents in SoC windows with high pressure gradients, triggers an inhomogeneous lithium distribution as well as a lithium salt concentration gradient and, therefore, significantly increases the risk of plating. These effects

do not occur during real-life applications with lower currents and long rest periods. Hence, in that case, increasing *stress factors* is not a sweet spot of acceleration, but triggers effects that do not occur in real-life applications.

This reversible capacity effect due to continuous cycling with high currents must be considered in AAM testing for hard case or externally fixed cells. Therefore, recovery strategies such as rest periods must be considered for appropriate lifetime estimates. Considering this effect can help to evaluate the actual influence of the initially applied offset pressure and the pressure gradient on AAM to find a clear causal relationship compared to the previous contradictory results. A precise understanding of the interplay of current rate, pressure and voltage gradients over SoC and optimised recovery strategies must be the scope of upcoming research to use AAM for lifetime prediction. However, if the pressure is not defined by a hard casing but is set via an external fixture, a rather constant pressure setup might be beneficial, as it impedes pressure gradients.

3.4. Potential of Post-Mortem Analysis for Accelerated Ageing Characterisation

Complementary to the previously discussed high precision measurement and accelerated ageing methods, various analysis techniques can offer additional insight into the chemical, electrochemical and morphological properties and components of a LIB. While penetrative imaging procedures, such as computed tomogratphy,[94,224] X-ray diffraction,[225,226] acoustic imaging[93,227] and neutron diffraction allow a non-destructive in-operando investigation, invasive methods usually require the opening of the tested cell in a post mortem analysis (PMA) excluding any further use of the cell.

In this section, we do not discuss analysis techniques as they can be found elsewhere,[13] but we provide case studies from the literature that demonstrate the power and limitations of invasive methods for accelerated ageing characterisation.

By conducting a PMA and comparing a pristine and an aged cell, invasive methods provide information about interactions of *stress factors* from AAM and HPM and the underlying *ageing mechanisms*. This knowledge can also be used to design physics-based ageing models which depict these interactions. Furthermore, invasive methods can ensure the transferability of accelerated ageing tests to the *unaccelerated reference*. The common relations between *ageing mechanisms* and *stress factors* are already discussed in the previous sections in numerous exemplary studies. Some of these studies,[16,17,142,178] among others, found a change in *ageing mechanisms* when the *stress factors* are tightened and thus help identify their limits for AAM.

The first case study by Jalkanen et al.[178] did a visual inspection of the components of pouch cells cycled at different temperatures (room temperature, 45 °C, 45 °C/65 °C). The alterations of the graphite anode, separator, and amount of residual electrolyte were similar but stronger with increasing temperature. However, the NMC cathode exhibited particle cracking and delamination only when cycling at 65 °C. Hence, an additional *ageing mechanism* has been triggered for 65 °C. Here, only PMA could reveal without a doubt that the doubling in ageing effects for the highest temperature is not due to valid acceleration but involved an additional *ageing mechanism*.

Watanabe et al.[240,241] used a combination of scanning electron microscopy, high-angle annular dark-field scanning transmission electron microscopy, tunnelling electron microscopy, and X-ray photoelectron spectroscopy to investigate the underlying processes for faster degradation of an lithium nickel cobalt aluminium oxides (NCA) cathode material under high DoD, high SoC and high-temperature operation. They concluded that microcracks in the secondary particle of the cathode are provoked solely by cycling with 100% DoD. For cycling with 60% DoD microcracking occurred neither in a low (10% to 70% SoC) nor in a high SoC regime (40% to 100% SoC). Consequently, NiO-like layers grow on the surface area exposed by the microcracks, leading to an isolation of the secondary particle and, hence, to the loss of active material. Further, they observed an increase in the growth rate of the NiO-like passivation layer with increasing temperature. This example shows, on the one hand, that PMA revealed an additional *ageing mechanism* as the *stress factor* (here DoD) is increased. On the other hand, PMA showed that the acceleration through an increase in temperature is valid: exactly the same *ageing mechanism* was enhanced as the thickness of the NiO-like layer increased from 8 nm for 25 °C to 25 nm for 60 °C.

In their study on the impact of porosity on the ageing of the silicon/graphite composite electrode material, Profatilova et al.[242] observed a faster capacity fade and resistance increase for cells with lower porosity at the full cell level. However, EIS spectra of coin cells harvested from the aged cells revealed no major differences in impedance between the cells with different porosities. Instead, pore-clogging of the separator caused by lithium plating is assumed to be the origin of resistance increase. They reasoned their findings by observing greyish precipitations on the separator and anode surface of the aged cells. Furthermore, X-ray photoelectron spectroscopy revealed a higher lithium concentration in the SEI of the anode with lower porosity compared to the one with higher porosity (57.4% vs. 38.6%) supporting the assumption of lithium plating.

Müller et al.[210] investigated stacked pouch cells with a NMC-811 cathode and Si/Gr blend as anode material at different levels of pressure (uncompressed, 0.08 MPa, 0.42 MPa and 0.84 MPa) as well as under fixed and flexible compression. In addition, an 18650 cylindrical cell with the same active material was assembled. After 100 cycles with constant current/constant voltage charge at C/3 and a 1C discharge, the negative electrodes and separators harvested from the stacked pouch cells were investigated by scanning electron microscopy. For cells under fixed compression, an average reduction in separator thickness was observed of roughly 20% compared to the pristine cells. Furthermore, the separator surfaces showed signs of penetration by the active materials, most likely due to volumetric expansions of the latter. Although pouch cells with fixed compression had a higher impedance increase and capacity fade than cells with flexible compression, their active

materials showed a higher remaining specific capacity when tested in a coin cell setup. Consequently, the authors concluded that the pore-clogging of the separator and the linked increase in resistance are the main reason for the observed capacity loss. These observations could also be made at different locations of the 18650 cylindrical jelly roll during PMA, as depicted in Figure Figure 11. Thereby, PMA not only revealed the impact of different pressure levels and fixation types for pouch cells, but also supported the understanding of which compression conditions are present at different locations in the jelly roll of an 18650 cylindrical cell.

Local dependencies in ageing were also observed by Keil et al.,[196] who conducted neutron diffraction experiments to investigate the dominant phases of active material during ageing experiments with 18650 cylindrical cells. From the difference in capacity determined through stochiometry of the neutron diffraction analysis and electrical analysis, they concluded more severe ageing at the edges of the jelly roll. Similar observations have been reported for pouch cells by Cai et al.,[243] who also used neutron diffraction to determine the dominant phases.

Although PMA is typically used for the analysis of aged cells, Schmid et al.[244] opened the cells at BoL, assembled coin cells, and analysed their ageing behaviour compared to the full cell setup. They showed that the correlation between *stress factors* and coin cell ageing can be transferred with certain restrictions to full cell ageing because the same *ageing mechanisms* and the same temperature dependency in ageing were observed. Although the coin cells degraded faster, this method is promising for accelerated ageing characterisation. In addition, the assembly of half cells allows to investigate the impact of *stress factors* on the each electrode individually, which is hardly possible for pure electrical testing in the original cell. Thereby, one could not only establish a finer granulated model but using coin cells further helps to identify which component is responsible for a given limitation when increasing a *stress factor*. Nevertheless, results can be falsified as other conditions, such as electrolyte composition, compression of active material, separator material, and lithium as counter-electrode, are present. For example, Schmid et al.[244] reported different levels of moisture intrusion depending on the choice of material for the sealing ring. Bridgewater et al.[245] observed different dominant ageing mechanisms for the same active material compositions but other cell formats.

Even so, both groups concluded a qualitative transferability between the ageing of the electrode material in the full cell and their coin cell setup.

Similar observations have been reported by Trask et al.,[246] who used the ageing of coin cells to evaluate and improve the lifetime performance of 400 mAh pouch cells. In conclusion, coin cell setup is a promising tool for identifying improvement potentials for different areas of material properties.

As highlighted in the previous examples, PMA is a valuable tool for the accelerated characterisation of ageing as a complement to electrically based HPM and AAM. The information gained from the analyses helps to understand the *ageing mechanisms* and their relationship to *stress factors* supporting electrochemical modelling.

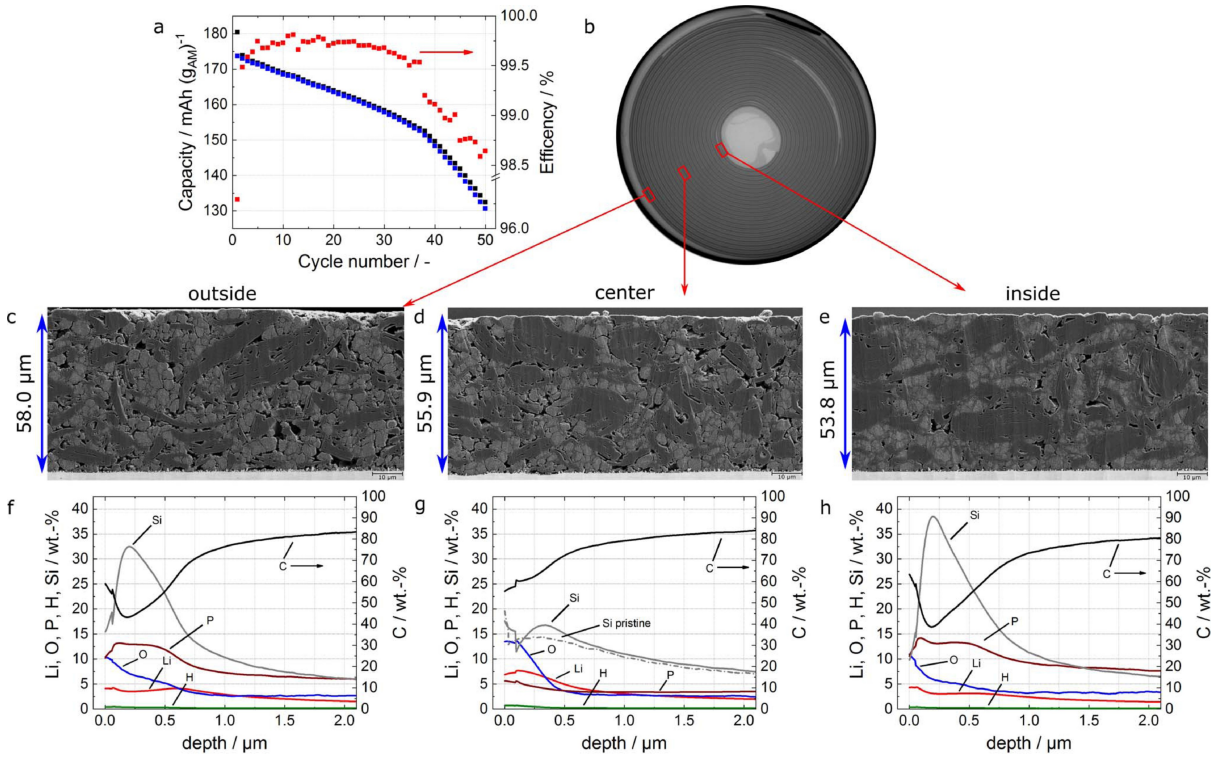

Figure 11. Müller et al.[210] investigated a cyclically aged 18650 cell (a) at different sections of the jelly roll (b). By using scanning electron microscopy (c-e) and GD-OES (f-h), they could observe spatially distributed ageing effects, which they ascribe to inhomogeneous compression occurring along the jelly roll. The graphic is reproduced from Müller et al.[210] under Creative Commons Attribution 4.0 license, CC BY.

Firstly, the effects of tightening the *stress factors* on *ageing mechanisms* can be identified by invasive methods. However, published research and data indicate that PMA does not allow easy conclusions about exact limits when *ageing mechanisms* change. As the test matrices only cover discrete conditions, the stress level at which another ageing mechanism occurs can only be approximated. Nevertheless, invasive investigation can answer whether specific *ageing mechanisms* have occurred or not.

Secondly, for the prediction of ageing and electrochemical modelling of ageing, the transfer between invasive and electrical methods is beneficial for validating models. PMA can provide accurate quantitative information on the *ageing mechanisms* that occurred. This helps accelerate lifetime prediction with consistent accuracy. Unfortunately, invasive methods are rarely carried out for ageing studies focusing on the quantitative correlation between *stress factors* and the observed *ageing mechanisms*, but mainly on a yes/no basis, i.e. whether specific effects occur. In addition, many references state that *ageing effects* are observed at a "high" or "low" stress factor but do not precisely define from which point a *stress factor* is "high" or "low".

As PMA or invasive analyses are usually conducted after the LIB reaches EoL and rarely during ageing tests, those links cannot be clearly described. Instead, the point of time for the conduction of PMA along an ageing study can only be estimated from literature and best knowledge. Thus, in the current state of research, it cannot be concluded from the literature at what time or SoH during ageing tests a PMA should be performed to identify ageing mechanisms as early as possible.

Assuming that the correlation of electrode properties, like porosity, and *ageing mechanisms* is thoroughly studied, and those properties are already known in advance, conclusions can be drawn about the susceptibility of cells to different *stress factors* as early as BoL.

Overall, invasive methods have great potential to link *ageing mechanisms* to the conditions during ageing and therefore help to accelerate the characterisation and prediction of ageing. However, enormous effort is required beforehand. Through smart design of experiment, not only the underlying *ageing mechanisms* can be identified, but also the progress of ageing in response to the *stress factors*.

3.5. Uncertainty in Cell Testing Methods: A Statistical Perspective

In general, a *model conception* aims at linking *stress factors* like temperature, current, and voltage with *ageing effects*, i.e. capacity fade and resistance increase with a general mathematical description. This can range from simple empirical models to more sophisticated physical models, statistical models, or machine learning approaches. A model is necessary to extrapolate the inferential results from the accelerated ageing experiments test data to normal operating conditions and to make real-world lifetime predictions based on these data. Basic *model conceptions* and mathematical/statistical methods developed for analysing the AAM experimental data are discussed in this section, organised by their objectives, structure, and fitting techniques, with the provided references being exemplary and by no means complete.

With respect to their main objectives, the available LIB research studies can be classified into one or more of the following three general categories.

- Lifetime estimation and prediction
- Stress factors and their effect analysis
- Ageing mechanism identification

Lifetime estimation and prediction: The works in this category aim to estimate the LIBs ageing over time (calendar tests), under cyclic usage (cycling) or both superimposed. The target is to approximate the ageing curve by using an *ageing variable* (e.g. time) as a predictor and to give early prediction of failure times (i.e. the time points at which the EoL criterion is met) at fixed levels of influential *stress factors*. Depending on the investigated problem, the ageing is quantified in various ways, for example, by capacity loss,[247] remaining useful lifetime,[248] end of performance,[249] SoH, or SoC.[250]

Stress factors and their effect analysis: Such studies try to determine *stress factors* with significant influence on ageing, such as temperature,[251] charge and discharge current rates,[239] SoC[36] and DoD,[170] and specify the exact *ageing trend* (e.g. capacity-stress dependence in cyclic ageing[252]) among different levels of the *stress factor*. Another objective is to examine the joint effect of different factors, i.e. developing a multi-factor ageing model.[47]

Ageing mechanism identification: Another possible goal is to identify and diagnose the *degradation modes* of a LIB at any point in its life.[46] This approach typically models the physicochemical degradation and provides a mechanistic understanding of capacity-fading processes and failure mechanisms.[95]

Numerous mathematical and statistical tools have been proposed depending on the main objective, the type of experiment, and the available data. For the *stress factors and their effect analysis*, most often nonlinear regression[24,230] or analysis of variance[47,252,253] models are applied, while *ageing mechanisms* are usually identified with the help of linear models[46] or physico empirical hybrid methods.[190] The model structure adopted in *lifetime estimation and prediction* is more complex, especially for cyclic tests, ranging from simple linear regression[219] to sigmoidal-type regression[254] and penalised regression (elastic net).[255] In general, we suggest the following classification of the modelling procedures used in the LIB literature:

- empirical models (e.g. a linear extrapolation method for approximating the normalised capacity in cyclic ageing under five stress factors,[256] and capacity fade in calendar ageing modelled by a function of time, consisting of an exponential and a linear part and with coefficients adjusted for temperature and SoC level combinations[65]),
- physical models (e.g. use of the Arrhenius law for the ageing-temperature dependence,[65] the Butler-Volmer equation for

the electrochemical kinetics,[257] the Fick's law for the flux of molecules[258] or the Palmgren-Miner rule[259]),

- hybrid approaches – combining empirical and physics based models (e.g. evolution of capacity and internal resistance models in calendar ageing[170,260] and a remaining useful life model in cyclic ageing by fusing empirical and statistical-based algorithms along with a relevance vector machine (RVM)[261]),
- statistical models and methods (e.g. Johnen et al.[254] propose a sigmoidal model for capacity degradation in cyclic ageing, introducing Gaussian errors and developing point and interval estimation for the parameters of the model, providing, beyond asymptotic, bootstrap estimation and prediction intervals for the capacity; Richardson et al.[262] adopt a Bayesian non-parametric approach using Gaussian process regression to predict capacity fade in calendar ageing under different usage scenarios),
- machine learning or broader artificial intelligence methods (e.g. capacity fade predictions by gradient boosting regression,[263] predictions of the remaining useful life by artificial neural networks (ANN) in cyclic ageing,[264] and a prediction model for cycle life with no knowledge of the *ageing mechanisms* but only based on a data set obtained under a variety of fast charging conditions[255]).

All of these different approaches have individual strengths and are useful for different purposes, without one being superior to the others. One challenge all models face is the variability of cells. Even if one model worked perfectly for a specific cell, it may fail for another. They all come with uncertainties that depend on the quality and amount of data used for fitting and parameterisa tion, as well as the objective.

In the sequel, we shall focus on statistical models since, under certain distribution assumptions, they account for uncertainties in estimating or predicting the *ageing effect* of interest (e.g. the capacity fade) caused by variability among LIBs in the testing sample, model adequacy, and other experimental-related factors. Thus, in contrast to the other methods, statistical-based approaches control the precision of estimations and predictions, providing, e.g. prediction intervals of a certain confidence level while allowing an assessment of the validity of the adopted models.

In both calendar and cyclic tests, the most commonly considered statistical approaches involve modelling the *ageing effect* as a function of the *ageing variable* by linear or non-linear regression. Polynomial models or models with exponential or logistic terms are usually suggested.[253,254] Such models are fitted using maximum likelihood estimation,[254] ordinary least squares[46] or non-linear least squares techniques.[53,170] Notice that procedures fitting empirical regression models by ordinary least squares assume Gaussian errors without always stating them.

In a parametric setup, the LIB lifetimes are modelled by fitting distributions. For example, Harris et al.[265] fit Weibull distributions, whereas Johnen et al.[254] examined the fit of Weibull, lognormal, and inverse Gaussian distributions, also considering the effect of a misspecified distributional assumption.

A frequently used non-parametric framework for modelling the degradation paths in calendar[262,266] and cyclic[263] tests is that of Gaussian processes, which accounts for the large variability in the LIB ageing paths.

Overall, special interest lies in investigating statistical models and procedures in terms of their ability to provide accurate predictions in the early experimental stages.[255,267]

The fitted models or adopted statistical procedures are statistically validated by suitable goodness-of-fit measures and tests, depending on their type. For instance, the coefficient of determination (R^2) is a very popular goodness-of-fit measure in linear regression,[170,181] tests based on *F*-ratio statistics are employed in analysis of variance models,[47,252] while Kolmogorov-Smirnov and Cramér-von-Mises goodness-of-fit tests can be applied to test the adequacy of a fitted distribution.[254]

However, every statistical test is valid only under specific assumptions. Thus, control of the underlying assumptions is always crucial, e.g. for the analysis of variance testing presented by Su et al.[47] Most of these tests are asymptotic, requiring a large sample size, which is rarely available in LIB experiments.

In such cases, simulation-based procedures are convenient alternatives (e.g. Johnen et al.[254] used bootstrap simulations). Bayesian procedures are another attractive option since they also allow the integration of prior information on the model parameters, based, e.g. on previous studies or experts' opinion, via a prior distribution.[268] The posterior distribution of the parameters can usually not be derived explicitly, but Markov chain Monte Carlo sampling schemes are developed to sample from it.[268–270] Furthermore, the predictive performance of the fitted models can be measured by cross-validation (CrossVal), based on the root mean squared error or mean absolute error.[255,267] In general, a straightforward comparison of results and models fitted on data observed or simulated under different experimental setups is rarely possible due to the effect of the differences in testing conditions, *stress factors*, their levels and combinations of these features. Thus, apart from using a Bayesian framework, it is hard to directly match results from different ageing studies and perform a statistical meta-analysis in the context of LIB testing.

In reliability theory, AAMs are additionally classified as accelerated life testing (ALT) or accelerated degradation testing (ADT).[271–273] The former models lifetimes with physical failures (hard failure), while the latter considers degradation paths of an ageing characteristic (e.g. SoH) that measures the *ageing effect*, with a failure defined as the characteristic exceeding a prespecified level of degradation (soft failure).[274] ADT experimental data contain observed paths of the ageing characteristic and are more informative than ALT data that contain only the observed failure times. Thus, ALT methods can be directly applied to ADT data by setting the hard failure according to a fixed EoL criterion, while the opposite is not possible. Hence, ADT modelling allows for flexibility in the specification of the EoL criterion. The analysis of ALT data is usually parametric,[254] whereas ADT can also be related to parametric models,[254] but is often based on stochastic processes.[263,266]

Nevertheless, in both ADT and ALT, life predictions are based on modelling the *ageing effect* either as a function of

only time (EFC)[254] or also incorporating additional *ageing/stress variables*.[169,247,275–277] Models of the first type are encoded in the literature as two-dimensional (2D), while the latter as *k*D (with $k > 2$).

Accelerated ageing tests are carried out under static (constant stress) or dynamic experimental conditions (e.g., Lucu et al.[266] consider both setups). The limitations of accelerating battery ageing have been discussed in Section 3.3.

In the case of 2D modelling, a model (link function) is required for the transferability of the predictions to the *unaccelerated reference*. Such a link function is based on physical models or is estimated by a regression-type model and commonly uses the superposition principle for the *ageing effect* in the dynamic setup, which might not hold in some cases. It is especially challenging to derive an estimation of the real-world lifetime using AAM tests with continuous cycling. This issue has not been considered in LIB testing (in a general ALT context, s. [279]).

In addition, it is worth mentioning that in AAMs quite often censoring can occur, usually due to time constraints (Type-I censoring) or by stopping the experiment when a pre-specified number of failures is obtained (Type-II censoring). However, there are only a few studies in the LIB literature dealing with Typel[267] or Type-II[265] censoring. Even less attention has been paid to the estimation procedures for experiments with interval-monitored data, as in the case of LIB data with RPT measurements (s. [254] for an exception).

Finally, another direction that shows the demand for further research is the statistical experimental design of LIB tests. Although the *modelling conception* does not directly accelerate cell ageing, it complements the corresponding AAM by producing lifetime predictions and/or extrapolating the results to the *unaccelerated reference* conditions. Thus, AAM tests must be carefully designed before being carried out to ensure the desired accuracy of the results. For example, the sample size determination is crucial, depends on the complexity of the model to be fitted, and affects the precision of the predictions. Thus, it needs to be carefully planned, e.g. Dechent et al.[270] considered the minimal number of tested cells required to estimate with desired precision the variability in LIB life due to the manufacturing process.

Using a hierarchical Bayesian approach, Dechent et al.[270] concluded that linear ageing models with 1 or 2 parameters require tests on at least 9 or 11 cells, respectively. In contrast, a three-parameter model with linear and exponential part should be fitted to measurements on at least 13 cells.

However, the *stress factors*, the number of their levels and the number of cells tested in each factor combination must be chosen appropriately. Moreover, in order to ensure model estimability, the sample size has to be adjusted according to the specific model structure. For example, the analysis of stress factors and their effects is commonly associated with experiments based on more testing conditions ($\geq$ 10) and a few measurements (1, 2 or 3) under each condition,[47,252] while machine learning and statistical Bayesian methods for capacity predictions require a large number of measurements ($\geq$ 100) in a single testing setup,[248,255,264] see Table 9.

To outline the relationship between the main objective of the experiment and the *modelling conception*, an overview of the major LIB testing and modelling aspects is presented in Table 9, where a selection of LIB studies is organised with respect to the ageing type, main objectives, modelling quantity, sample size and modelling approach of the studies.

4. Conclusions

In this review, we approached the superordinate question of how fast ageing behaviour can be determined in ageing tests and estimated over the lifetime. It is essential to distinguish between the acceleration of the ageing characterisation and the acceleration of the battery ageing itself. Therefore, we separated the accelerated ageing characterisation into two *acceleration techniques*, namely high precision measurement (HPM) and accelerated ageing method (AAM). Both aim to accelerate the ageing characterisation while battery ageing is only accelerated by AAM.

Using HPM, the low ageing during the first cycles or storage days without altering stress factors requires a high-precision measurement. Moreover, a model for extrapolating the data and compensating for reversible effects, such as the anode overhang effect, which has a strong impact at the beginning of the test. Therefore, the two promising methods FCA and HPC must be carried out under ideal load and environmental conditions, leading to higher requirements for the test hardware and peripherals. Transferability to the *unaccelerated reference* is generally given due to the low *stress factors*.

In contrast, for AAM, the accelerating momentum when tightening the *stress factors* needs to be known to transfer the results of the accelerated tests to the *unaccelerated reference* and to get as close as possible to the *sweet spot* of acceleration. The suitability of *stress factors* to accelerate ageing was discussed for SoC, temperature, C-rate, pressure and continuous cycling for calendar and cyclic ageing and is summarised as follows:

- SoC: Calendar ageing is accelerated with increasing SoC with a *sweet spot* between 60% 90%. Cyclic ageing is accelerated at high and low SoC when cycling between transition stages of the graphite. Thus, accelerated testing should be performed in a potential window containing a graphite transition stage. At high SoC from about 80% *ageing mechanisms* at the cathode are triggered.
- Temperature: The acceleration for increasing the temperature is generally quantified by the Arrhenius relation, both for calendar and cyclic ageing. Compared to other stress factors, it is relatively easy to identify the limits of acceleration in this regard. At around 45 °C, the dominant *ageing mechanisms* change, while the maximum temperature acceleration is exceeded above 60 °C when thermal instabilities start to occur. For cyclic ageing and towards low temperatures, the anode degradation is accelerated, which results in minimum ageing at around 30 °C.
- C-rate: Testing with a higher C-rate has two effects. Firstly, it accelerates the testing as more EFC are reached in the same

amount of time. Secondly, higher C-rates enhance the occurring ageing mechanisms as current-induced mechanical stresses due to (de-)intercalation processes increase. However, the interdependencies with resistance, heat generation, temperature, and ageing must be considered as they can cause the ageing to decelerate even at a higher C-rate. Further, it has to be distinguished between charging and discharging current rates.

- Testing without Resting: In order to reduce measurement time, cells are often cycled continuously at high C-rates while rest periods are eliminated compared to the *unaccelerated reference*. In combination with pronounced pressure gradients over SoC, high apparent capacity loss is observable, which can be recovered during subsequent rest periods. This effect is so far associated with compressed cells. The compression cannot be avoided in most applications and has to be considered for not overestimating the ageing compared to the *unaccelerated reference* with long rest periods and lower C-rates.

In contrast to AAM, predictive characterisation conducted at BoL provides insights into potential *ageing effects* and *degradation modes*, aiding in accelerated degradation analysis without extensive test matrices and time-consuming RPTs.

In addition to electrochemical characterisation, alternative methods like thickness and pressure measurements or isothermal calorimetry are valuable tools that can support the ageing characterisation. After cells have gone through AAM or HPM ageing, invasive methods complement the characterisation, since they verify the *consistency* in the *ageing mechanisms* and thus the *transferability* of accelerated testing to the unaccelerated reference.

In addition to the discussed experimental methods, careful data evaluation is crucial considering effects due to the measurement itself and the reversible capacity. Furthermore, a *model conception* is vital for lifetime prediction. Depending on the sample size, test duration, and cell ageing variability, statistical methods allow evaluating estimation precision and prediction accuracy. Including prior knowledge of cell ageing behaviour in such models reduces the necessary equipment and time.

In general, much time and effort are saved when the experimental design and the modelling approach are constructed based on the objective of the accelerated study (e.g. lifetime estimation, stress effect analysis, or ageing mechanism identification) and side effects are considered.

Overall, there is no one and only test strategy for accelerated ageing characterisation and no universal answer to the questions raised initially. Identified trends and limits are rarely valid across the board. They can mainly be identified for individual groups of cells, such as specific cell chemistries or high-power and highenergy cells, when comprehensive experimental ageing studies are conducted and evaluated carefully. Thus, this review summarises strategies to accelerate ageing characterisation, gives a comprehensive overview of possible approaches along with their advantages and disadvantages, and points out aspects that need to be considered before and during testing as well as for data analysis. Therefore, it provides guidance for the challenges associated with the accelerated ageing characterisation of lithium-ion batteries.

Acknowledgements

The research is funded by the German Federal Ministry of Education and Research, within the project BALd in the Cluster BattNutzung, Grant Nr. 03XP0320A to E.

Philipp Dechent and Sabine Paarmann are currently funded by the Deutsche Forschungsgemeinschaft (DFG, German Research Foundation) – 506629963; 511349305.

We thank the reviewers for their exceptional and constructive review, one of them Paul Gasper, National Renewable Energy Laboratory (NREL). Open Access funding enabled and organized by Projekt DEAL.

Conflict of Interests

The authors declare no conflict of interest.

Data Availability Statement

Data sharing is not applicable to this article as no new data were created or analyzed in this study.

Keywords: accelerated ageing methods · ageing mechanisms · electrochemistry · energy conversion · high precision measurements

[1] G. Pistoia, B. Liaw, *Behaviour of Lithium-Ion Batteries in Electric Vehicles*, Springer International Publishing, Cham **2018**.
[2] J. E. Harlow, X. Ma, J. Li, E. Logan, Y. Liu, N. Zhang, L. Ma, S. L. Glazier, M. M. E. Cormier, M. Genovese, S. Buteau, A. Cameron, J. E. Stark, J. R. Dahn, *J. Electrochem. Soc.* **2019**, *166*, A3031.
[3] N. Wassiliadis, M. Steinsträter, M. Schreiber, P. Rosner, L. Nicoletti, F. Schmid, M. Ank, O. Teichert, L. Wildfeuer, J. Schneider, A. Koch, A. König, A. Glatz, J. Gandlgruber, T. Kröger, X. Lin, M. Lienkamp, *eTransportation* **2022**, *12*, 100167.
[4] H.-H. Braess, U. Seiffert, *Vieweg Handbuch Kraftfahrzeugtechnik*, Springer Fachmedien Wiesbaden, Wiesbaden **2021**.
[5] A. Masias, J. Marcicki, W. A. Paxton, *ACS Energy Lett.* **2021**, *6*, 621.
[6] Peter Slowik, Aaron Isenstadt, Logan Pierce, Stephanie Searle **2022**.
[7] J. Vetter, P. Novák, M. R. Wagner, C. Veit, K.-C. Möller, J. O. Besenhard, M. Winter, M. Wohlfahrt-Mehrens, C. Vogler, A. Hammouche, *J. Power Sources* **2005**, *147*, 269.
[8] J. S. Edge, S. O'Kane, R. Prosser, N. D. Kirkaldy, A. N. Patel, A. Hales, A. Ghosh, W. Ai, J. Chen, J. Yang, S. Li, M.-C. Pang, L. Bravo Diaz, A. Tomaszewska, M. W. Marzook, K. N. Radhakrishnan, H. Wang, Y. Patel, B. Wu, G. J. Offer, *Phys. Chem. Chem. Phys.* **2021**, *23*, 8200.
[9] P. M. Attia, A. Bills, F. B. Planella, P. Dechent, G. d. Reis, M. Dubarry, P. Gasper, R. Gilchrist, S. Greenbank, D. Howey, O. Liu, E. Khoo, Y. Preger, A. Soni, S. Sripad, A. G. Stefanopoulou, V. Sulzer, PREPRINT "Knees" in lithium-ion battery aging trajectories.
[10] X. Han, L. Lu, Y. Zheng, X. Feng, Z. Li, J. Li, M. Ouyang, *eTransportation* **2019**, *1*, 100005.
[11] T. Waldmann, B.-I. Hogg, M. Wohlfahrt-Mehrens, *J. Power Sources* **2018**, *384*, 107.
[12] C. Pastor-Fernández, T. F. Yu, W. D. Widanage, J. Marco, *Renewable Sustainable Energy Rev.* **2019**, *109*, 138.

[13] T. Waldmann, A. Iturrondobeitia, M. Kasper, N. Ghanbari, F. Aguesse, E. Bekaert, L. Daniel, S. Genies, I. J. Gordon, M. W. Löble, E. de Vito, M. Wohlfahrt-Mehrens, *J. Electrochem. Soc.* **2016**, *163*, A2149.
[14] P. Iurilli, C. Brivio, V. Wood, *J. Power Sources* **2021**, *505*, 229860.
[15] R. Li, W. Li, A. Singh, D. Ren, Z. Hou, M. Ouyang, *Energy Storage Mater.* **2022**, *52*, 395.
[16] M. Alipour, C. Ziebert, F. V. Conte, R. Kizilel, *Batteries* **2020**, *6*, 35.
[17] A. Tomaszewska, Z. Chu, X. Feng, S. O'Kane, X. Liu, J. Chen, C. Ji, E. Endler, R. Li, L. Liu, Y. Li, S. Zheng, S. Vetterlein, M. Gao, J. Du, M. Parkes, M. Ouyang, M. Marinescu, G. Offer, B. Wu, *eTransportation* **2019**, *1*, 100011.
[18] J. Jaguemont, L. Boulon, Y. Dubé, *Appl. Energy* **2016**, *164*, 99.
[19] N. Collath, B. Tepe, S. Englberger, A. Jossen, H. Hesse, *J. Energy Storage* **2022**, *55*, 105634.
[20] Y. Gao, X. Zhang, Q. Cheng, B. Guo, J. Yang, *IEEE Access* **2019**, *7*, 43511.
[21] N. Wassiliadis, J. Schneider, A. Frank, L. Wildfeuer, X. Lin, A. Jossen, M. Lienkamp, *J. Energy Storage* **2021**, *44*, 103306.
[22] A. Eddahech, O. Briat, J.-M. Vinassa, *Electrochim. Acta* **2013**, *114*, 750.
[23] E. Wikner, E. Björklund, J. Fridner, D. Brandell, T. Thiringer, *J. Power Sources Advances* **2021**, *8*, 100054.
[24] W. Diao, S. Saxena, M. Pecht, *J. Power Sources* **2019**, *435*, 226830.
[25] E. Sarasketa-Zabala, I. Gandiaga, L. M. Rodriguez-Martinez, I. Villarreal, *J. Power Sources* **2014**, *272*, 45.
[26] New vehicle limited warranty: Model S, Model X, Model 3, Model Y **22.03.2021**.
[27] Garantie für Hochvoltbatterien für BEV und PHEV-Fahrzeuge der Volkswagen AG **05/2019**.
[28] C. R. Birkl, M. R. Roberts, E. McTurk, P. G. Bruce, D. A. Howey, *J. Power Sources* **2017**, *341*, 373.
[29] X. Ma, J. E. Harlow, J. Li, L. Ma, D. S. Hall, S. Buteau, M. Genovese, M. Cormier, J. R. Dahn, *J. Electrochem. Soc.* **2019**, *166*.
[30] W. Diao, S. Saxena, B. Han, M. Pecht, *Energies* **2019**, *12*, 2910.
[31] C. Strange, S. Li, R. Gilchrist, G. dos Reis, *Energies* **2021**, *14*, 1206.
[32] J. de Hoog, J.-M. Timmermans, D. loan-Stroe, M. Swierczynski, J. Jaguemont, S. Goutam, N. Omar, J. van Mierlo, P. van den Bossche, *Appl. Energy* **2017**, *200*, 47.
[33] M. Swierczynski, D.-I. Stroe, A.-I. Stan, R. Teodorescu, S. K. Kær, *IEEE Trans. Ind. Appl.* **2015**, *Vol. 51*, pp. 3453.
[34] S. Atalay, M. Sheikh, A. Mariani, Y. Merla, E. Bower, W. D. Widanage, *J. Power Sources* **2020**, *478*, 229026.
[35] M. Simolka, J.-F. Heger, H. Kaess, I. Biswas, K. A. Friedrich, *J. Appl. Electrochem.* **2020**, *50*, 1101.
[36] J. Schmalstieg, S. Käbitz, M. Ecker, D. U. Sauer, *J. Power Sources* **2014**, *257*, 325.
[37] C. Nobis, T. Kuhnimhof, Mobilität in Deutschland MiD Ergebnisbericht.
[38] J. B. Goodenough, Y. Kim, *Chem. Mater.* **2010**, *22*, 587.
[39] T. Guan, P. Zuo, S. Sun, C. Du, L. Zhang, Y. Cui, L. Yang, Y. Gao, G. Yin, F. Wang, *J. Power Sources* **2014**, *268*, 816.
[40] J. C. Burns, A. Kassam, N. N. Sinha, L. E. Downie, L. Solnickova, B. M. Way, J. R. Dahn, *J. Electrochem. Soc.* **2013**, *160*, A1451.
[41] C. Zhang, Y. Wang, Y. Gao, F. Wang, B. Mu, W. Zhang, *Appl. Energy* **2019**, *256*, 113841.
[42] Y. Preger, H. M. Barkholtz, A. Fresquez, D. L. Campbell, B. W. Juba, J. Romàn-Kustas, S. R. Ferreira, B. Chalamala, *J. Electrochem. Soc.* **2020**, *167*, 120532.
[43] P. Gasper, A. Saxon, Y. Shi, E. Endler, K. Smith, F. M. Thakkar, *J. Energy Storage* **2023**, *73*, 109042.
[44] G. Pozzato, A. Allam, L. Pulvirenti, G. A. Negoita, W. A. Paxton, S. Onori, *Joule* **2023**.
[45] K. Smith, P. Gasper, A. M. Colclasure, Y. Shimonishi, S. Yoshida, *J. Electrochem. Soc.* **2021**, *168*, 100530.
[46] Y. Gao, S. Yang, J. Jiang, C. Zhang, W. Zhang, X. Zhou, *J. Electrochem. Soc.* **2019**, *166*, A1623.
[47] L. Su, J. Zhang, C. Wang, Y. Zhang, Z. Li, Y. Song, T. Jin, Z. Ma, *Appl. Energy* **2016**, *163*, 201.
[48] M. Lewerenz, S. Käbitz, M. Knips, J. Münnix, J. Schmalstieg, A. Warnecke, D. U. Sauer, *J. Power Sources* **2017**, *353*, 144.
[49] M. Lewerenz, G. Fuchs, L. Becker, D. U. Sauer, *J. Energy Storage* **2018**, *18*, 149.
[50] T. Hüfner, M. Oldenburger, B. Bedürftig, A. Gruhle, *J. Energy Storage* **2019**, *24*, 100790.
[51] J. Wilhelm, S. Seidlmayer, P. Keil, J. Schuster, A. Kriele, R. Gilles, A. Jossen, *J. Power Sources* **2017**, *365*, 327.
[52] M. Azzam, M. Ehrensberger, R. Scheuer, C. Endisch, M. Lewerenz, *Energies* **2023**, page 3889.
[53] S. Käbitz, J. B. Gerschler, M. Ecker, Y. Yurdagel, B. Emmermacher, D. André, T. Mitsch, D. U. Sauer, *J. Power Sources* **2013**, *239*, 572.
[54] M. Lewerenz, P. Dechent, D. U. Sauer, *J. Energy Storage* **2019**, *21*, 680.
[55] G. Ngaleu, M. Theiler, X. Straßer, C. Hanzl, L. Komsiyska, C. Endisch, M. Lewerenz, *Batteries* **2022**, *8*, 33.
[56] X. Strasser, G. Ngaleu, C. Hanzl, M. Azzam, C. Endisch, M. Lewerenz, *Batteries* **2023**.
[57] M. Rogge, A. Jossen, *Batteries & Supercaps* **2023**, *n/a*, e202300313.
[58] B. Gyenes, D. A. Stevens, V. L. Chevrier, J. R. Dahn, *J. Electrochem. Soc.* **2015**, *162*, A278.
[59] T. Bank, L. Alsheimer, N. Löffler, D. U. Sauer, *J. Energy Storage* **2022**, *51*, 104201.
[60] F. Hildenbrand, D. Ditscheid, E. Barbers, D. U. Sauer, *Appl. Energy* **2023**, *332*, 120395.
[61] J. P. Fath, L. Alsheimer, M. Storch, J. Stadler, J. Bandlow, S. Hahn, R. Riedel, T. Wetzel, *J. Energy Storage* **2020**, *29*, 101344.
[62] F. Röder, S. Ramasubramanian, *Energy Technol.* **2022**, *10*.
[63] T. Raj, A. A. Wang, C. W. Monroe, D. A. Howey, *Batteries & Supercaps* **2020**, *3*, 1377.
[64] K. L. Gering, S. V. Sazhin, D. K. Jamison, C. J. Michelbacher, B. Y. Liaw, M. Dubarry, M. Cugnet, *J. Power Sources* **2011**, *196*, 3395.
[65] D. Werner, S. Paarmann, T. Wetzel, *Batteries* **2021**, *7*, 28.
[66] L. Su, J. Zhang, J. Huang, H. Ge, Z. Li, F. Xie, B. Y. Liaw, *J. Power Sources* **2016**, *315*, 35.
[67] A. Karger, L. Wildfeuer, D. Aygül, A. Maheshwari, J. P. Singer, A. Jossen, *J. Energy Storage* **2022**, *52*, 104718.
[68] E. Redondo-Iglesias, P. Venet, S. Pelissier, *Batteries* **2020**, *6*, 14.
[69] A. Adamson, K. Tuul, T. Bötticher, S. Azam, M. D. L. Garayt, M. Metzger, *Nat. Mater.* **2023**, *22*, 1380–1386.
[70] G. Mulder, N. Omar, S. Pauwels, F. Leemans, B. Verbrugge, W. de Nijs, P. van den Bossche, D. Six, J. van Mierlo, *J. Power Sources* **2011**, *196*, 10079.
[71] A. Barai, K. Uddin, M. Dubarry, L. Somerville, A. McGordon, P. Jennings, I. Bloom, *Prog. Energy Combust. Sci.* **2019**, *72*, 1.
[72] J. C. Burns, N. N. Sinha, G. Jain, H. Ye, C. M. VanElzen, W. M. Lamanna, A. Xiao, E. Scott, J. Choi, J. R. Dahn, *J. Electrochem. Soc.* **2012**, *159*, A1105.
[73] F. Hildenbrand, F. Aupperle, G. Stahl, E. Figgmeier, D. U. Sauer, *Batteries & Supercaps* **2022**, *5*.
[74] C. Jin, H. Li, Y. Song, B. Lu, A. K. Soh, J. Zhang, *Science China Technological Sciences* **2019**, *62*, 1357.
[75] P. Dechent, E. Barbers, A. Epp, D. Jöst, W. Li, D. U. Sauer, S. Lehner, *Energy Technol.* **2023**.
[76] Y. Wu, P. Keil, S. F. Schuster, A. Jossen, *J. Electrochem. Soc.* **2017**, *164*, A1438.
[77] D. Werner, S. Paarmann, A. Wiebelt, T. Wetzel, *Batteries* **2020**, *6*, 13.
[78] P. Kuntz, O. Raccurt, P. Azaïs, K. Richter, T. Waldmann, M. Wohlfahrt-Mehrens, M. Bardet, A. Buzlukov, S. Genies, *Batteries* **2021**, *7*, 48.
[79] I. Bloom, S. A. Jones, V. S. Battaglia, G. L. Henriksen, J. P. Christophersen, R. B. Wright, C. D. Ho, J. R. Belt, C. G. Motloch, *J. Power Sources* **2003**, *124*, 538.
[80] Y. Zhang, C.-Y. Wang, X. Tang, *J. Power Sources* **2011**, *196*, 1513.
[81] B. Epding, B. Rumberg, H. Jahnke, I. Stradtmann, A. Kwade, *J. Energy Storage* **2019**, *22*, 249.
[82] P. Dechent, A. Epp, D. Jöst, Y. Preger, P. M. Attia, W. Li, D. U. Sauer, *ACS Energy Lett.* **2021**, *6*, 2351.
[83] A. Louli, L. Ellis, J. Dahn, *Joule* **2019**, *3*, 745–761.
[84] S. Paarmann, K. Schuld, T. Wetzel, *Energy Technol.* **2022**, page 2200384.
[85] N. A. Samad, Y. Kim, J. B. Siegel, A. G. Stefanopoulou, *J. Electrochem. Soc.* **2016**, *163*, A1584–A1594.
[86] P. Mohtat, S. Lee, J. B. Siegel, A. G. Stefanopoulou, *J. Electrochem. Soc.* **2021**, *168*, 100520.
[87] L. Kong, R. Aalund, M. Alipour, S. I. Stoliarov, M. Pecht, *J. Electrochem. Soc.* **2022**, *169*, 040541.
[88] T. Baumhöfer, M. Brühl, S. Rothgang, D. U. Sauer, *J. Power Sources* **2014**, *247*, 332.
[89] D. Beck, P. Dechent, M. Junker, D. U. Sauer, M. Dubarry, *Energies* **2021**, *14*, 3276.
[90] S. K. Rechkemmer, X. Zang, W. Zhang, O. Sawodny, *J. Energy Storage* **2020**, *30*, 101547.
[91] M. Dubarry, C. Truchot, M. Cugnet, B. Y. Liaw, K. Gering, S. Sazhin, D. Jamison, C. Michelbacher, *J. Power Sources* **2011**, *196*, 10328.
[92] K. Rumpf, M. Naumann, A. Jossen, *J. Energy Storage* **2017**, *14*, 224.
[93] D. Wasylowski, N. Kisseler, H. Ditler, M. Sonnet, G. Fuchs, F. Ringbeck, D. U. Sauer, *J. Power Sources* **2022**, *521*, 230825.

[94] M. Spielbauer, P. Berg, J. Soellner, J. Peters, F. Schaeufl, C. Rosenmüller, O. Bohlen, A. Jossen, *J. Energy Storage* **2021**, *43*, 103213.
[95] M. Dubarry, C. Truchot, B. Y. Liaw, *J. Power Sources* **2012**, *219*, 204.
[96] M.-T. F. Rodrigues, *J. Electrochem. Soc.* **2022**, *169*, 080524.
[97] A. J. Smith, H. M. Dahn, J. C. Burns, J. R. Dahn, *J. Electrochem. Soc.* **2012**, *159*, A705.
[98] A. Chahbaz, F. Meishner, W. Li, C. Ünlübayir, D. Uwe Sauer, *Energy Storage Mater.* **2021**, *42*, 794.
[99] A. Weng, J. B. Siegel, A. Stefanopoulou, *Front. Energy Res.* **2023**, *11*.
[100] R. Tian, S.-H. Park, P. J. King, G. Cunningham, J. Coelho, V. Nicolosi, J. N. Coleman, *Nat. Commun.* **2019**, *10*, 1933.
[101] C. Heubner, K. Nikolowski, S. Reuber, M. Schneider, M. Wolter, A. Michaelis, *Batteries & Supercaps* **2021**, *4*, 268.
[102] F. Single, B. Horstmann, A. Latz, *J. Phys. Chem. C* **2019**, *123*, 27327.
[103] P. Shafiei Sabet, D. U. Sauer, *J. Power Sources* **2019**, *425*, 121.
[104] W. Waag, S. Käbitz, D. U. Sauer, *Appl. Energy* **2013**, *102*, 885.
[105] H. Zappen, F. Ringbeck, D. Sauer, *Batteries* **2018**, *4*, 64.
[106] M. Schindler, J. Sturm, S. Ludwig, J. Schmitt, A. Jossen, *eTransportation* **2021**, *8*, 100102.
[107] J. C. Burns, R. Petibon, K. J. Nelson, N. N. Sinha, A. Kassam, B. M. Way, J. R. Dahn, *J. Electrochem. Soc.* **2013**, *160*, A1668.
[108] L. Bläubaum, F. Röder, C. Nowak, H. S. Chan, A. Kwade, U. Krewer, *ChemElectroChem* **2020**, *7*, 4755.
[109] A. Weng, P. Mohtat, P. M. Attia, V. Sulzer, S. Lee, G. Less, A. Stefanopoulou, *Joule* **2021**, *5*, 2971.
[110] I. A. Profatilova, S.-S. Kim, N.-S. Choi, *Electrochim. Acta* **2009**, *54*, 4445.
[111] E. R. Logan, H. Hebecker, X. Ma, J. Quinn, Y. HyeJeong, S. Kumakura, J. Paulsen, J. R. Dahn, *J. Electrochem. Soc.* **2020**, *167*, 060530.
[112] X. Zeng, G.-L. Xu, Y. Li, X. Luo, F. Maglia, C. Bauer, S. F. Lux, O. Paschos, S.-J. Kim, P. Lamp, J. Lu, K. Amine, Z. Chen, *ACS Appl. Mater. Interfaces* **2016**, *8*, 3446.
[113] T. Deutschen, S. Gasser, M. Schaller, J. Siehr, *J. Energy Storage* **2018**, *19*, 113.
[114] M. Lewerenz, J. Münnix, J. Schmalstieg, S. Käbitz, M. Knips, D. U. Sauer, *J. Power Sources* **2017**, *345*, 254.
[115] L. Streck, T. Roth, P. Keil, B. Strehle, S. Ludmann, A. Jossen, *J. Electrochem. Soc.* **2023**, *170*, 040520.
[116] S. Glazier, *Isothermal microcalorimetry as a tool to probe parasitic reactions in lithium-ion cells* **2018**.
[117] T. Roth, L. Streck, A. Graule, P. Niehoff, A. Jossen, *J. Electrochem. Soc.* **2023**, *170*, 020502.
[118] Michael Theiler, Christian Endisch and Meinert Lewerenz, *Batteries* **2021**, pages 7,22.
[119] M. C. Schulze, M.-T. F. Rodrigues, J. D. McBrayer, D. P. Abraham, C. A. Apblett, I. Bloom, Z. Chen, A. M. Colclasure, A. R. Dunlop, C. Fang, K. L. Harrison, G. Liu, S. D. Minteer, N. R. Neale, D. Robertson, A. P. Tornheim, S. E. Trask, G. M. Veith, A. Verma, Z. Yang, C. Johnson, *J. Electrochem. Soc.* **2022**, *169*, 050531.
[120] S. M. P. Jagfeld, K. P. Birke, A. Fill, P. Keil, *Batteries* **2023**, *9*, 232.
[121] M. Azzam, C. Endisch, M. Lewerenz, *Batteries* **2024**, *10*, 3.
[122] P. Keil, A. Jossen, *J. Electrochem. Soc.* **2017**, *164*, A3081.
[123] B. Rumberg, B. Epding, I. Stradtmann, M. Schleder, A. Kwade, *J. Energy Storage* **2020**, *30*, 101510.
[124] T. Boetticher, A. Adamson, S. Buechele, E. D. Alter, M. Metzger, *J. Electrochem. Soc.* **2023**, *170*, 060507.
[125] A. Verma, M. C. Schulze, A. Colclasure, M.-T. F. Rodrigues, S. E. Trask, K. Pupek, C. S. Johnson, D. P. Abraham, *J. Electrochem. Soc.* **2023**, *170*, 070516.
[126] A. J. Smith, J. C. Burns, S. Trussler, J. R. Dahn, *J. Electrochem. Soc.* **2010**, *157*, A196.
[127] A. J. Smith, J. C. Burns, D. Xiong, J. R. Dahn, *J. Electrochem. Soc.* **2011**, *158*, A1136.
[128] R. Fathi, J. C. Burns, D. A. Stevens, H. Ye, C. Hu, G. Jain, E. Scott, C. Schmidt, J. R. Dahn, *J. Electrochem. Soc.* **2014**, *161*, A1572.
[129] A. Fly, B. Wimarshana, I. Bin-Mat-Arishad, M. Sarmiento-Carnevali, *J. Energy Storage* **2022**, *52*, 104721.
[130] A. J. Smith, J. C. Burns, J. R. Dahn, *Electrochem. Solid-State Lett.* **2010**, *13*, A177.
[131] N. N. Sinha, A. J. Smith, J. C. Burns, G. Jain, K. W. Eberman, E. Scott, J. P. Gardner, J. R. Dahn, *J. Electrochem. Soc.* **2011**, *158*, A1194.
[132] J. C. Burns, G. Jain, A. J. Smith, K. W. Eberman, E. Scott, J. P. Gardner, J. R. Dahn, *J. Electrochem. Soc.* **2011**, *158*, A255.
[133] T. M. Bond, J. C. Burns, D. A. Stevens, H. M. Dahn, J. R. Dahn, *J. Electrochem. Soc.* **2013**, *160*, A521.
[134] A. J. Smith, J. C. Burns, X. Zhao, D. Xiong, J. R. Dahn, *J. Electrochem. Soc.* **2011**, *158*, A447.
[135] P. Keil, A. Jossen, *J. Electrochem. Soc.* **2017**, *164*, A6066.
[136] A. Zülke, Y. Li, P. Keil, H. Hoster, *J. Electrochem. Soc.* **2019**, *166*, A2921.
[137] S. L. Glazier, S. A. Odom, A. P. Kaur, J. R. Dahn, *J. Electrochem. Soc.* **2018**, *165*, A3449–A3458.
[138] E. R. Logan, J. R. Dahn, *J. Electrochem. Soc.* **2021**, *168*, 120526.
[139] E. R. Logan, A. J. Louli, M. Genovese, S. Trussler, J. R. Dahn, *J. Electrochem. Soc.* **2021**, *168*, 060527.
[140] A. Eldesoky, E. R. Logan, A. J. Louli, W. Song, R. Weber, S. Hy, R. Petibon, J. E. Harlow, S. Azam, E. Zsoldos, J. R. Dahn, *J. Electrochem. Soc.* **2022**, *169*, 010501.
[141] W.-Y. Chang, *International Scholarly Research Notices* **2013**.
[142] M. Broussely, P. Biensan, F. Bonhomme, P. Blanchard, S. Herreyre, K. Nechev, R. J. Staniewicz, *J. Power Sources* **2005**, *146*, 90.
[143] S. Oswald, H. A. Gasteiger, *J. Electrochem. Soc.* **2023**, *170*, 030506.
[144] M. Wohlfahrt-Mehrens, C. Vogler, J. Garche, *J. Power Sources* **2004**, *127*, 58.
[145] B. Stiaszny, J. C. Ziegler, E. E. Krauß, M. Zhang, J. P. Schmidt, E. Ivers-Tiffée, *J. Power Sources* **2014**, *258*, 61.
[146] F. Schipper, E. M. Erickson, C. Erk, J.-Y. Shin, F. F. Chesneau, D. Aurbach, *J. Electrochem. Soc.* **2017**, *164*, A6220.
[147] B. Scrosati, J. Garche, *J. Power Sources* **2010**, *195*, 2419.
[148] S. J. An, J. Li, C. Daniel, D. Mohanty, S. Nagpure, D. L. Wood, *Carbon* **2016**, *105*, 52.
[149] H. Zhang, Y. Yang, D. Ren, L. Wang, X. He, *Energy Storage Mater.* **2021**, *36*, 147.
[150] R. Yazami, Y. F. Reynier, *Electrochim. Acta* **2002**, *47*, 1217.
[151] L. Spitthoff, P. R. Shearing, O. S. Burheim, *Energies* **2021**, *14*, 1248.
[152] L. Wildfeuer, A. Karger, D. Aygül, N. Wassiliadis, A. Jossen, M. Lienkamp, *J. Power Sources* **2023**, *560*, 232498.
[153] M. Broussely, S. Herreyre, P. Biensan, P. Kasztejna, K. Nechev, R. Staniewicz, *J. Power Sources* **2001**, *97–98*, 13.
[154] H. J. Ploehn, P. Ramadass, R. E. White, *J. Electrochem. Soc.* **2004**, *151*, A456.
[155] P. M. Attia, W. C. Chueh, S. J. Harris, *J. Electrochem. Soc.* **2020**, *167*, 090535.
[156] P. Keil, S. F. Schuster, J. Wilhelm, J. Travi, A. Hauser, R. C. Karl, A. Jossen, *J. Electrochem. Soc.* **2016**, *163*, A1872.
[157] J. Jiang, Y. Gao, C. Zhang, W. Zhang, Y. Jiang, *J. Electrochem. Soc.* **2019**, *166*, A1070.
[158] M. Lewerenz, A. Marongiu, A. Warnecke, D. U. Sauer, *J. Power Sources* **2017**, *368*, 57.
[159] S. Schweidler, L. de Biasi, A. Schiele, P. Hartmann, T. Brezesinski, J. Janek, *J. Phys. Chem. C* **2018**, *122*, 8829.
[160] N. Lin, Z. Jia, Z. Wang, H. Zhao, G. Ai, X. Song, Y. Bai, V. Battaglia, C. Sun, J. Qiao, K. Wu, G. Liu, *J. Power Sources* **2017**, *365*, 235.
[161] M. Koltypin, Y. S. Cohen, B. Markovsky, Y. Cohen, D. Aurbach, *Electrochem. Commun.* **2002**, *4*, 17.
[162] A. Mikheenkova, A. J. Smith, K. B. Frenander, Y. Tesfamhret, N. R. Chowdhury, C.-W. Tai, T. Thiringer, R. W. Lindström, M. Hahlin, M. J. Lacey, *J. Electrochem. Soc.* **2023**, *170*, 080503.
[163] N. R. Chowdhury, A. J. Smith, K. Frenander, A. Mikheenkova, R. W. Lindström, T. Thiringer, *J. Energy Storage* **2024**, *76*, 110001.
[164] N. Kirkaldy, M. A. Samieian, G. J. Offer, M. Marinescu, Y. Patel, *ACS Appl. Energ. Mater.* **2022**, *5*, 13367.
[165] C. Xu, K. Märker, J. Lee, A. Mahadevegowda, P. J. Reeves, S. J. Day, M. F. Groh, S. P. Emge, C. Ducati, B. Layla Mehdi, C. C. Tang, C. P. Grey, *Nat. Mater.* **2021**, *20*, 84.
[166] Y. Ruan, X. Song, Y. Fu, C. Song, V. Battaglia, *J. Power Sources* **2018**, *400*, 539.
[167] B. Stiaszny, J. C. Ziegler, E. E. Krauß, J. P. Schmidt, E. Ivers-Tiffée, *J. Power Sources* **2014**, *251*, 439.
[168] F. B. Spingler, M. Naumann, A. Jossen, *J. Electrochem. Soc.* **2020**, *167*, 040526.
[169] M. Naumann, F. B. Spingler, A. Jossen, *J. Power Sources* **2020**, *451*, 227666.
[170] M. Ecker, J. B. Gerschler, J. Vogel, S. Käbitz, F. Hust, P. Dechent, D. U. Sauer, *J. Power Sources* **2012**, *215*, 248.
[171] E. Cuervo-Reyes, R. Flückiger, *J. Electrochem. Soc.* **2019**, *166*, A1463.
[172] P. Verma, P. Maire, P. Novák, *Electrochim. Acta* **2010**, *55*, 6332.
[173] X. Feng, M. Ouyang, X. Liu, L. Lu, Y. Xia, X. He, *Energy Storage Mater.* **2018**, *10*, 246.
[174] K. Tuul, S. M. Maher, C. Floras, W. Black, T. Taskovic, S. Chisholm, A. Clarke, E. Lust, J. R. Dahn, *J. Electrochem. Soc.* **2024**, *171*, 040510.

[175] J. Tarascon, D. Guyomard, *Solid State Ionics* **1994**, *69*, 293.
[176] T. Waldmann, G. Bisle, B.-I. Hogg, S. Stumpp, M. A. Danzer, M. Kasper, P. Axmann, M. Wohlfahrt-Mehrens, *J. Electrochem. Soc.* **2015**, *162*, A921.
[177] L. Tan, L. Zhang, Q. Sun, M. Shen, Q. Qu, H. Zheng, *Electrochim. Acta* **2013**, *111*, 802.
[178] K. Jalkanen, J. Karppinen, L. Skogström, T. Laurila, M. Nisula, K. Vuorilehto, *Appl. Energy* **2015**, *154*, 160.
[179] W. Agyei Appiah, J. Park, S. Byun, Y. Roh, M. H. Ryou, Y. M. Lee, *ChemElectroChem* **2019**, *6*, 3714.
[180] J. Wang, P. Liu, J. Hicks-Garner, E. Sherman, S. Soukiazian, M. Verbrugge, H. Tataria, J. Musser, P. Finamore, *J. Power Sources* **2011**, *196*, 3942.
[181] T. Waldmann, M. Wilka, M. Kasper, M. Fleischhammer, M. Wohlfahrt-Mehrens, *J. Power Sources* **2014**, *262*, 129.
[182] M. Schimpe, M. Edler von Kuepach, M. Naumann, H. C. Hesse, K. Smith, A. Jossen, *ECS Trans.* **2018**, *80*, 147.
[183] G. Kucinskis, M. Bozorgchenani, M. Feinauer, M. Kasper, M. Wohlfahrt-Mehrens, T. Waldmann, *J. Power Sources* **2022**, *549*, 232129.
[184] D. Werner, S. Paarmann, A. Wiebelt, T. Wetzel, *Batteries* **2020**, *6*, 12.
[185] V. Ruiz, A. Kriston, I. Adanouj, M. Destro, D. Fontana, A. Pfrang, *Electrochim. Acta* **2017**, *240*, 495.
[186] eTech49, #52 | Interview Dr Greg Offer, Imperial College London, Battery Technology **2021**.
[187] I. A. Hunt, Y. Zhao, Y. Patel, J. Offer, *J. Electrochem. Soc.* **2016**, *163*, A1846.
[188] J. Fleckenstein, O. Bohlen, B. Bäker, *World Electric Vehicle Journal* **2012**.
[189] R. Carter, T. A. Kingston, R. W. Atkinson, M. Parmananda, M. Dubarry, C. Fear, P. P. Mukherjee, C. T. Love, *Cell Rep. Phy. Sci.* **2021**, *2*, 100351.
[190] R. Carter, E. J. Klein, T. A. Kingston, C. T. Love, *Front. Energy Res.* **2019**, *7*.
[191] J. Wang, J. Purewal, P. Liu, J. Hicks-Garner, S. Soukazian, E. Sherman, A. Sorenson, L. Vu, H. Tataria, M. W. Verbrugge, *J. Power Sources* **2014**, *269*, 937.
[192] S. Sun, T. Guan, X. Cheng, P. Zuo, Y. Gao, C. Du, G. Yin, *RSC Adv.* **2018**, *8*, 25695.
[193] J. Christensen, J. Newman, *J. Solid State Electrochem.* **2006**, *10*, 293.
[194] M. B. Pinson, M. Z. Bazant, *J. Electrochem. Soc.* **2013**, *160*, A243.
[195] S. F. Schuster, T. Bach, E. Fleder, J. Müller, M. Brand, G. Sextl, A. Jossen, *J. Energy Storage* **2015**, *1*, 44.
[196] J. Keil, N. Paul, V. Baran, P. Keil, R. Gilles, A. Jossen, *J. Electrochem. Soc.* **2019**, *166*, A3908.
[197] C. Wang, T. Amietszajew, R. Carvajal, Y. Guo, Z. Ahmed, C. Zhang, G. Goodlet, R. Bhagat, *Energies* **2021**, *14*, 4724.
[198] S. Barcellona, L. Piegari, *J. Energy Storage* **2020**, *29*, 101310.
[199] P. Morales Torricos, C. Endisch, M. Lewerenz, *Batteries* **2023**, *9*, 230.
[200] T. C. Bach, S. F. Schuster, E. Fleder, J. Müller, M. J. Brand, H. Lorrmann, A. Jossen, G. Sextl, *J. Energy Storage* **2016**, *5*, 212.
[201] P. M. Attia, S. Das, S. J. Harris, M. Z. Bazant, W. C. Chueh, *J. Electrochem. Soc.* **2019**, *166*, E97–E106.
[202] S. Das, P. M. Attia, W. C. Chueh, M. Z. Bazant, *J. Electrochem. Soc.* **2019**, *166*, E107–E118.
[203] A. Weng, E. Olide, I. Kovalchuk, J. B. Siegel, A. Stefanopoulou, *J. Electrochem. Soc.* **2023**, *170*, 090523.
[204] T. Waldmann, M. Kasper, M. Wohlfahrt Mehrens, *Electrochim. Acta* **2015**, *178*, 525.
[205] J. Cannarella, C. B. Arnold, *J. Power Sources* **2014**, *245*, 745.
[206] A. Barai, R. Tangirala, K. Uddin, J. Chevalier, Y. Guo, A. McGordon, P. Jennings, *J. Energy Storage* **2017**, *13*, 211.
[207] Y. H. Choi, H. K. Lim, J.-H. Seo, W. J. Shin, J. H. Choi, J. H. Park, *SAE Intern. J. Altern. Powertrains* **2018**, *7*, 195.
[208] M. Wünsch, J. Kaufman, D. U. Sauer, *Journal of Energy Storage* **2019**, *21*, 149.
[209] A. Barai, G. Yue, A. McGordon, P. Jennings, *A Study of the Effects of External Pressure on the Electrical Performance of a Lithiumion Pouch Cell*, IEEE, Piscataway, NJ **2013**.
[210] V. Müller, R.-G. Scurtu, K. Richter, T. Waldmann, M. Memm, M. A. Danzer, M. WohlfahrtMehrens, *J. Electrochem. Soc.* **2019**, *166*, A3796.
[211] J. Zhang, *Int. J. Electrochem. Sci.* **2020**, pages 8422–8436.
[212] T. Deich, M. Storch, K. Steiner, A. Bund, *J. Power Sources* **2021**, *506*, 230163.
[213] M. Lewerenz, C. Rahe, G. Fuchs, C. Endisch, D. U. Sauer, *J. Energy Storage* **2020**, *30*, 101529.
[214] Alexander Alan Holland.
[215] A. J. Smith, Y. Fang, A. Mikheenkova, H. Ekström, P. Svens, I. Ahmed, M. J. Lacey, G. Lindbergh, I. Furó, R. W. Lindström, *J. Power Sources* **2023**, *573*, 233118.
[216] J. Stadler, T. K. Groch, M. García, M. Storch, J. Fath, M. Ecker, A. Latz, *J. Energy Storage* **2023**, *65*, 107247.
[217] E. Sarasketa-Zabala, I. Gandiaga, E. MartinezLaserna, L. M. Rodriguez-Martinez, I. Villarreal, *J. Power Sources* **2015**, *275*, 573.
[218] M. Lewerenz, D. U. Sauer, *J. Energy Storage* **2018**, *18*, 421.
[219] M. Ecker, N. Nieto, S. Käbitz, J. Schmalstieg, H. Blanke, A. Warnecke, D. U. Sauer, *J. Power Sources* **2014**, *248*, 839.
[220] J. Cannarella, C. B. Arnold, *J. Electrochem. Soc.* **2015**, pages A1365–A1373.
[221] M. Lewerenz, A. Warnecke, D. U. Sauer, *J. Power Sources* **2017**, *354*, 157.
[222] N. S. Nazer, M. Strobl, A. Kaestner, P. J. Vie, V. A. Yartys, *Electrochim. Acta* **2022**, *427*, 140793.
[223] C. P. Aiken, N. Kowalski, R. C. Fitzner, S. Trussler, J. E. Harlow, E. J. Butler, J. R. Dahn, *J. Electrochem. Soc.* **2023**, *170*, 040529.
[224] L. Willenberg, P. Dechent, G. Fuchs, M. Teuber, M. Eckert, M. Graff, N. Kürten, D. U. Sauer, E. Figgemeier, *J. Electrochem. Soc.* **2020**, *167*, 120502.
[225] T. R. Tanim, P. P. Paul, V. Thampy, C. Cao, H.-G. Steinrück, J. Nelson Weker, M. F. Toney, E. J. Dufek, M. C. Evans, A. N. Jansen, B. J. Polzin, A. R. Dunlop, S. E. Trask, *Cell Rep. Phys. Sci.* **2020**, *1*, 100114.
[226] D. Liu, Z. Shadike, R. Lin, K. Qian, H. Li, K. Li, S. Wang, Q. Yu, M. Liu, S. Ganapathy, X. Qin, Q.-H. Yang, M. Wagemaker, F. Kang, X.-Q. Yang, B. Li, *Advanced materials (Deerfield Beach, Fla.)* **2019**, *31*, e1806620.
[227] G. Davies, K. W. Knehr, B. Van Tassell, T. Hodson, S. Biswas, A. G. Hsieh, D. A. Steingart, *J. Electrochem. Soc.* **2017**, *164*, A2746–A2755.
[228] J. Belt, V. Utgikar, I. Bloom, *J. Power Sources* **2011**, *196*, 10213.
[229] M. Kassem, J. Bernard, R. Revel, S. Pélissier, F. Duclaud, C. Delacourt, *J. Power Sources* **2012**, *208*, 296.
[230] Y. Gao, J. Jiang, C. Zhang, W. Zhang, Y. Jiang, *J. Power Sources* **2018**, *400*, 641.
[231] J. Zhu, M. Knapp, D. R. Sørensen, M. Heere, M. S. Darma, M. Müller, L. Mereacre, H. Dai, A. Senyshyn, X. Wei, H. Ehrenberg, *J. Power Sources* **2021**, *489*, 229422.
[232] S. Gantenbein, M. Schönleber, M. Weiss, E. Ivers-Tiffée, *Sustainability* **2019**, *11*, 6697.
[233] Y. Zhang, R. Xiong, H. He, X. Qu, M. Pecht, *Appl. Energy* **2019**, *255*, 113818.
[234] R. Gauthier, A. Luscombe, T. Bond, M. Bauer, M. Johnson, J. Harlow, A. Louli, J. R. Dahn, *J. Electrochem. Soc.* **2022**.
[235] T. Bank, J. Feldmann, S. Klamor, S. Bihn, D. U. Sauer, *J. Power Sources* **2020**, *473*, 228566.
[236] T. Nemeth, P. Schröer, M. Kuipers, D. U. Sauer, *J. Energy Storage* **2020**, *31*, 101656.
[237] L. Spitthoff, M. S. Wahl, J. J. Lamb, P. R. Shearing, P. J. S. Vie, O. S. Burheim, *Batteries* **2023**, *9*, 249.
[238] F. Leng, C. M. Tan, M. Pecht, *Sci. Rep.* **2015**, *5*, 12967.
[239] M. Dubarry, C. Truchot, B. Y. Liaw, *J. Power Sources* **2014**, *258*, 408.
[240] S. Watanabe, M. Kinoshita, T. Hosokawa, K. Morigaki, K. Nakura, *J. Power Sources* **2014**, *260*, 50.
[241] S. Watanabe, M. Kinoshita, T. Hosokawa, K. Morigaki, K. Nakura, *J. Power Sources* **2014**, *258*, 210.
[242] I. Profatilova, E. de Vito, S. Genies, C. Vincens, E. Gutel, O. Fanget, A. Martin, M. Chandesris, M. Tulodziecki, W. Porcher, *ACS Appl. Energ. Mater.* **2020**, *3*, 11873.
[243] L. Cai, K. An, Z. Feng, C. Liang, S. J. Harris, *J. Power Sources* **2013**, *236*, 163.
[244] A. U. Schmid, A. Ridder, M. Hahn, K. Schofer, K. P. Birke, *Batteries* **2020**, *6*, 33.
[245] G. Bridgewater, M. J. Capener, J. Brandon, M. J. Lain, M. Copley, E. Kendrick, *Batteries* **2021**, *7*, 38.
[246] S. E. Trask, Y. Li, J. J. Kubal, M. Bettge, B. J. Polzin, Y. Zhu, A. N. Jansen, D. P. Abraham, *J. Power Sources* **2014**, *259*, 233.
[247] E. Sarasketa-Zabala, E. Martinez-Laserna, M. Berecibar, I. Gandiaga, L. M. RodriguezMartinez, I. Villarreal, *Appl. Energy* **2016**, *162*, 839.
[248] X. Xu, C. Yu, S. Tang, X. Sun, X. Si, L. Wu, *Energies* **2019**, *12*, 1685.
[249] Y.-F. Wang, S.-T. Tseng, B. H. Lindqvist, K.-L. Tsui, *J. Quality Techn.* **2019**, *51*, 198.
[250] W. Yan, B. Zhang, G. Zhao, S. Tang, G. Niu, X. Wang, *IEEE Transactions on Industrial Electronics* **2019**, *66*, 3227.
[251] W. Diao, Y. Xing, S. Saxena, M. Pecht, *Appl. Sci.* **2018**, *8*, 1786.
[252] T. Gewald, A. Candussio, L. Wildfeuer, D. Lehmkuhl, A. Hahn, M. Lienkamp, *Batteries* **2020**, *6*, 6.

[253] M. Dubarry, A. Devie, *J. Energy Storage* **2018**, *18*, 185.
[254] M. Johnen, S. Pitzen, U. Kamps, M. Kateri, P. Dechent, D. U. Sauer, *J. Energy Storage* **2021**, *34*, 102011.
[255] K. A. Severson, P. M. Attia, N. Jin, N. Perkins, B. Jiang, Z. Yang, M. H. Chen, M. Aykol, P. K. Herring, D. Fraggedakis, M. Z. Bazant, S. J. Harris, W. C. Chueh, R. D. Braatz, *Nat. Energy* **2019**, *4*, 383.
[256] K. Takei, Y. Kumai, H. Kobayashi, H. Miyashiro, N. Terada, T. Iwahori, T. Tanaka, *J. Power Sources* **2001**.
[257] L. von Kolzenberg, J. Stadler, J. Fath, M. Ecker, B. Horstmann, A. Latz, *J. Power Sources* **2022**, *539*, 231560.
[258] S. E. O'Kane, W. Ai, G. Madabattula, D. Alonso-Alvarez, R. Timms, V. Sulzer, J. S. Edge, B. Wu, G. J. Offer, M. Marinescu, *Phys. Chem. Chem. Phys.* **2022**, *24*, 7909.
[259] L. Serrao, S. Onori, G. Rizzoni, Y. Guezennec, *IFAC Proc. Vol.* **2009**, *42*, 923.
[260] M. Montaru, S. Fiette, J.-L. Koné, Y. Bultel, *J. Energy Storage* **2022**, *51*, 104544.
[261] Y. Chang, H. Fang, Y. Zhang, *Appl. Energy* **2017**, *206*, 1564.
[262] R. R. Richardson, M. A. Osborne, D. A. Howey, *J. Energy Storage* **2019**, *23*, 320.
[263] R. R. Richardson, M. A. Osborne, D. A. Howey, *J. Power Sources* **2017**, *357*, 209.
[264] B. Long, X. Li, X. Gao, Z. Liu, *Energies* **2019**, *12*, 3271.
[265] S. J. Harris, D. J. Harris, C. Li, *J. Power Sources* **2017**, *342*, 589.
[266] M. Lucu, E. Martinez-Laserna, I. Gandiaga, K. Liu, H. Camblong, W. D. Widanage, J. Marco, *J. Energy Storage* **2020**, *30*, 101409.
[267] M. Johnen, C. Schmitz, M. Kateri, U. Kamps, *Computers and Industrial Engineering* **2020**, *143*, 106418.
[268] A. El Mejdoubi, H. Chaoui, H. Gualous, P. van den Bossche, N. Omar, J. van Mierlo, *IEEE Transactions on Power Electronics* **2019**, *34*, 6834.
[269] Z. Liu, A. Ivanco, S. Onori, *J. Energy Storage* **2019**, *21*, 519.
[270] P. Dechent, S. Greenbank, F. Hildenbrand, S. Jbabdi, D. U. Sauer, D. A. Howey, *Batteries & Supercaps* **2021**, *4*, 1821.
[271] L. A. Escobar, W. Q. Meeker, *Sta. Sci.* **2006**, *21*, 552.
[272] W. Q. Meeker, L. A. Escobar, C. J. Lu, *Technomet* **1998**, *40*, 89.
[273] W. B. Nelson, *Accelerated Life Testing: Statistical Models, Test Plans and Data Analyses*, Wiley, New York **1990**.
[274] P. W. Srivastava (Editor), *Optimum Accelerated Life Testing Models with Time-Varying Stresses*, WORLD SCIENTIFIC **2017**.
[275] E. Thomas, I. Bloom, J. Christophersen, V. Battaglia, *Journal of Power Sources* **2008**, *184*, 312.
[276] E. Thomas, I. Bloom, J. Christophersen, V. Battaglia, *Journal of Power Sources* **2012**, *206*, 378.
[277] P. Gasper, N. Collath, H. C. Hesse, A. Jossen, K. Smith, *Journal of The Electrochemical Society* **2022**, *169*, 080518.
[278] D.-I. Stroe, M. Swierczynski, A.-I. Stan, R. Teodorescu, S. J. Andreasen, *IEEE Transactions on Industry Applications* **2014**, *50*, 4006.
[279] T. Seiche, U. Kamps, *IEEE Transactions on Reliability* **2021**, *70*, 525.

Manuscript received: December 14, 2023
Revised manuscript received: June 7, 2024
Version of record online: ■■, ■■

REVIEW

Ageing characterisation of lithium-ion batteries needs to be accelerated compared to real-world applications to obtain ageing patterns in a short period of time. In this review, we discuss characterisation of fast ageing without triggering unintended ageing mechanisms and the required test duration for reliable lifetime prediction.

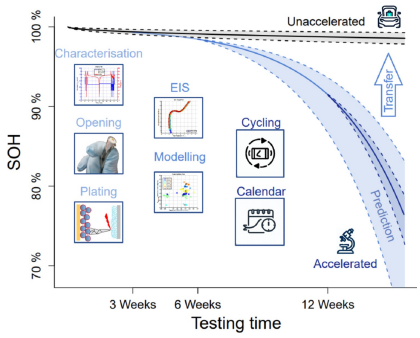

Dr.-Ing. S. Paarmann, M. Schreiber, A. Chahbaz, F. Hildenbrand, G. Stahl, M. Rogge, Dr.-Ing. P. Dechent, O. Queisser, S. D. Frankl, P. Morales Torricos, Y. Lu, Dr. N. I. Nikolov, Prof. M. Kateri, Prof. D. U. Sauer, Prof. M. A. Danzer, Prof. T. Wetzel, Prof. C. Endisch, Prof. M. Lienkamp, Prof. A. Jossen, Dr. M. Lewerenz*

1 – 38

Short-Term Tests, Long-Term Predictions – Accelerating Ageing Characterisation of Lithium-Ion Batteries